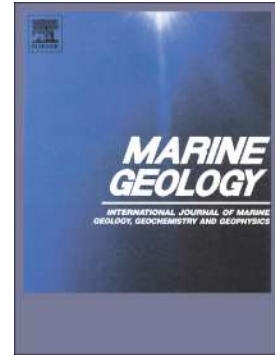# Journal Pre-proof

The sines contourite depositional system along the SW Portuguese margin: Onset, evolution and conceptual implications

S. Rodrigues, C. Roque, F.J. Hernández-Molina, E. Llave, P. Terrinha

Please cite this article as: S. Rodrigues, C. Roque, F.J. Hernández-Molina, et al., The sines contourite depositional system along the SW Portuguese margin: Onset, evolution and conceptual implications, *Marine Geology* (2020), https://doi.org/10.1016/j.margeo.2020.106357

The Sines Contourite Depositional System along the SW Portuguese Margin: onset, evolution and conceptual implications

Rodrigues, S.[1], Roque, C.[2,3], Hernández-Molina, F.J.[1], Llave, E.[4], Terrinha, P.[2,5]

[1] *Dept. Earth Sciences, Royal Holloway Univ. of London, Egham, Surrey TW20 0EX, UK,*

[2] *IDL-Instituto Dom Luiz, Faculdade de Ciências da Universidade de Lisboa, Campo Grande Edifício C1, 1749-016 Lisbon, Portugal,*

[3] *EMEPC-Estrutura de Missão para a Extensão da Plataforma Continental, Rua Costa Pinto 165, 2770-047 Paço de Arcos, Portugal,*

[4] *IGME-Instituto Geológico y Minero de España, Calle de Ríos Rosas 23, 28003 Madrid, Spain,*

[5] *IPMA-Instituto Português do Mar e da Atmosfera, Divisão de Geologia Marinha e Georecursos Marinhos, Rua C do Aeroporto 1749-077 Lisbon, Portugal*

Corresponding author: *Sara.Rodrigues.2017@live.rhul.ac.uk*

Abstract

The Sines Contourite Depositional System, located in the Southwest Portuguese Margin, is a central segment of the Iberian Contourite Depositional Complex, built under the influence of the Mediterranean Outflow Water (MOW). This work presents the onset and evolution of this system using multibeam bathymetry, multichannel seismic reflection lines, sediment cores and well data. Six seismic units of Late Miocene through Holocene age have been identified which defined three evolutionary stages for drift construction: a) an *onset* and *initial stage,* from the Late Miocene to the Late Pliocene (5.33 – 2.5 Ma), where a sheeted drift was built under a weak flowing MOW; b) a *growing stage* from the Early to Middle Quaternary (2.5 – 0.7 Ma), characterized by the deposition of a mounded drift in the south and a sheeted drift in the north, which is correlated with a strengthening of the MOW; and c) a *maintenance stage* between the Middle Pleistocene and Holocene (0.7 Ma – present), where the modern depositional and erosional contourite features developed associated with three intensification periods of the MOW at 0.7 Ma, 0.4 Ma and 20 ka. The development of the Sines Contourite Depositional System was constrained in the long-term by seafloor paleomorphologies inherited from the Mesozoic rifting phases of the Southwest Portuguese Margin. The NNW-SSE horsts and grabens built during the Mesozoic rifting provided accommodation for drift growth with limited lateral migration, and locally enhanced the alongslope bottom-current. In short-term, environmental (climate and sea-level) fluctuations modulated changes in bottom-current density and intensity, determining sedimentary cycles in the depositional record, especially during the Quaternary. Our findings emphasize the occurrence of three main plastered morphologies throughout the seismic record, which were compared with other plastered drifts in different continental margins to establish a conceptual model.

Keywords: *contourites, Sines Drift, Southwest Portuguese Margin, seismic analysis, IODP Expedition 339, Mediterranean Outflow Water*

1. Introduction

Contourite drifts have long been recognized along several continental margins, built under the influence of bottom-currents. Contourite deposition often involves multi-phase entrainment, long distance transport and interaction among sedimentary processes induced by a semi-permanent alongslope current over a long period of time (McCave, 2008; Stow *et al*., 2008). Thus, these features can provide long- and short-term sedimentary records for paleoceanographic and paleoclimatic fluctuations (Van Rooij *et al*., 2010; Llave *et al*., 2011; Pellegrini *et al*., 2016).

1

It is generally accepted that contourite drifts can be classified based on their overall geometry and location, however, overlap and gradation exists between all drift types (Faugères *et al.* ,1999; Stow and Faugères, 2008; Rebesco *et al*., 2014). The most common depositional features are large elongated drifts, with well-known examples for detached and separate drifts (Hunter *et al*., 2007a,b; Roque *et al*., 2012; Hernández-Molina *et al*., 2014, 2016b). While detached drifts show a predominant downslope progradation due to sediment deposition deviating away from the adjacent slope, separate drifts show upslope progradation due to alongslope deposition towards the slope (Faugères *et al*., 1999, Rebesco and Stow, 2001; Rebesco, 2005). However, there is a third type of large drifts along continental margins, which show considerable variation in sediment deposition: plastered drifts. Plastered drifts are characterized as a type of sheeted drift, elongated parallel to the slope with sediment deposition on one or both sides. They can therefore show both downslope and upslope migration (Faugères et al., 1999, Rebesco and Stow, 2001; Rebesco, 2005). Thus, their morphologies and stacking patterns provide a unique record for bottom-current variations in terms of intensity, pathway, and interaction with the slope gradient and seafloor irregularities.

In general, plastered drifts do not occur isolated. These features are linked to other depositional or erosional contourite features, such as sediment waves, terraces, moats or contourite channels. Genetically linked features establish a contourite depositional system (CDS), or a contourite depositional complex (CDC) if the CDS is distinct but built under the influence of the same water mass (Hernández-Molina *et al*., 2003, 2006).

An extensive CDC has been built around the Iberian Peninsula, under the influence of the Mediterranean Outflow Water (MOW). The CDC is characterized by six main CDS, from south to north: the Gulf of Cadiz, West Portuguese, Sines, Galicia, Ortegal and Le Danois CDS. These systems have been targeted by several works since the 1980's due to their complex nature (e.g., Faugères *et al*., 1985a, 1985b; Nelson *et al*., 1993, 1999; Llave *et al*., 2001, 2007, 2018, 2019; Hernández-Molina *et al*., 2006, 2014, 2016b; Van Rooij *et al*., 2010; Ercilla *et al*., 2011; Bender *et al*., 2012; Roque *et al*., 2012 and references herein). Distinct contourite features occur within each CDS, however giant elongated drifts are the most common.

MOW dynamics are responsible for building the Iberian CDC after the opening of the Strait of Gibraltar and the end of the Messinian Salinity Crisis (5.33 to 5.96 Ma ago) (Cita, 2001; Bache *et al*., 2012). The Gulf of Cadiz CDS corresponds to the most notorious example, with the Huelva, Faro,

2

Bartolomeus Dias, Guadalquivir, Albufeira, Portimão, Lagos and Sagres drifts (e.g. Vanney and Mougenot, 1981; Nelson *et al.*, 1993, 1999; Llave *et al.*, 2001, 2006, 2007, 2011, 2015, 2019; Hernández-Molina *et al.,* 2006, 2011, 2014, 2016b; Roque *et al.*, 2012). By contrast, the West Portuguese CDS and the Sines CDS hold the less known and studied contourite drifts.

The Sines Drift represents the main contourite depositional feature on the Sines CDS (Llave *et al.*, 2019; Teixeira *et al.*, 2019). The Sines Drift corresponds to a plastered drift formed along the middle continental slope of the SW Portuguese Margin, between 750 and 1800 m water depth (Fig. 1). Mougenot (1976) was the first author to identify the Sines Drift, based on seismic reflection lines and samples of seabed sediments. Other works by Alves *et al.* (2000, 2003) and Pereira and Alves (2010, 2011, 2013) focused on the long-term stratigraphic record for the older pre-rift and syn-rift sequences of the SW Portuguese Margin. Recently, it was drilled during the Integrated Ocean Drilling Program (IODP) Expedition 339 (Expedition 339 Scientists, 2012; Stow *et al.*, 2013; Hernández-Molina *et al.*, 2014, 2016b). Several ongoing works have focused on the potential impact of contourites and bottom-currents on slope stability (Neves *et al.*, 2016; Teixeira *et al.*, 2019) and on the interplay of deep-water processes along submarine canyons (Serra *et al.*, 2020), nearby slope scarps (Teixeira *et al.*, 2019) and on the formation of mixed contourite-turbidite deposits (Mencaroni *et al.*, 2020). These works have taken into consideration the evolution of the modern morphological and structural features, however the action and effect of bottom currents and climatic changes have been described only at a millennial scale (up to 42 ky BP in Teixeira *et al.*, 2020) and until the Late Pliocene (at 3.2 Ma in Teixeira *et al.*, 2019 and Mencaroni *et al.*, 2020). The previous works have yet to study the onset, evolutionary phases and sedimentary processes involved in the depositional history of the Sines CDS, considering that its formation begun in the Late Miocene (Rodrigues, 2017). The Sines CDS offers a key area to investigate plastered drifts in detail and a new perspective on their lateral (space) and vertical (time) variability. Thus, the main objectives of this work are: a) to establish an integrated study of the Sines CDS, determining its onset and evolutionary stages; b) to propose a sedimentary model for its evolution and decode the main controlling mechanisms involved in its formation, and c) to evaluate the vertical and lateral changes on the Sines plastered drift and develop the conceptual knowledge on this type of contourite drift and its complex sedimentary stacking pattern.

2. Geological and Oceanographic settings

3

2.1. Geologic setting

The SW Portuguese Margin is considered a type of non-volcanic asymmetric rift margin (Pinheiro *et al*., 1996; Tucholke *et al*., 2007). This margin began to develop during the early stages of continental rifting, from the Triassic to the Early Cretaceous, which led to the opening of the North Atlantic Ocean (Rasmussen *et al*., 1998; Alves *et al*., 2002, 2006, 2009, 2013; Pereira and Alves, 2010, 2011; Ribeiro, 2013; Terrinha *et al*., 2013a, 2013b). This process begun with the thinning of the continental lithosphere, which created NE-SW to NW-SE graben and half-graben structures and deposition of evaporites and continental deposits in the Late Triassic (Hettangian) (Azerêdo *et al*., 2003). This stage was followed by whole lithospheric rupture until the Early Cretaceous, which accommodated the initial formation of oceanic lithosphere and the development of a passive margin by Aptian-Albian times (Pereira and Alves, 2010, 2011). At the end of the Cenomanian, a change in the trajectory of Africa relative to Eurasia from NW-SE to SW-NE (Dewey *et al*., 1989; Srivastava *et al*., 1990; Ribeiro, 2013) provoked the rotation of Iberia and collision with Eurasia and Africa, forming the Pyrenean orogen in the Eocene, with the first compressive impulses registered in the Late Cretaceous (De Vicente *et al*., 2011). The continued convergence of Africa and Iberia during the Neogene led to the formation of the Betic orogen (De Vicente *et al*., 2011; Cunha *et al*., 2012). The SW Portuguese Margin is located near the Africa-Eurasia plate boundary, thus subjected to the remote effects of the collision and compression events during the Late Miocene (Mougenot *et al*., 1979; Ribeiro *et al*., 1990; Alves *et al.,* 2003, 2006; Pereira and Alves, 2011, 2013). These collision events caused the closure of the Rifian and Betic oceanic gateways between the Atlantic and the Mediterranean from ~7 to 6.1 Ma ago (Hsü *et al*., 1973; Sierro *et al*., 2008; Flecker *et al*., 2015; Capella *et al*., 2018), which led to the progressive isolation of the Mediterranean region (Hsü *et al*., 1978; Duggen *et al.*, 2003) and the Messinian Salinity Crisis between 5.96 and 5.33 Ma (Cita, 2001; Bache *et al*., 2012). In the Late Miocene, the extensional regime changed to an oblique NW-SE convergence (Dewey *et al*., 1989; Ribeiro *et al*., 1990; Terrinha *et al*., 2003) while the collapse of the Betic-Rif orogenic front occurred, probably associated with westward roll-back subduction of an oceanic lithosphere slab beneath the Gibraltar Arc and development of its accretionary wedge (Gutscher *et al*., 2002, 2012; Duarte *et al*., 2013). During this last period, a transtensional regime induced the reopening of the connection between the Atlantic and the Mediterranean through the Strait of Gibraltar, putting an end to the Messinian Salinity Crisis (Maldonado *et al*., 1999; Duggen *et al*., 2003; Garcia-Castellanos *et al.*, 2009).

The SW Portuguese Margin evolved towards more stable conditions during Pliocene and Quaternary times (Nelson *et al*., 1993, 1999; Maldonado *et al*., 1999; Somoza *et al*., 1999; Medialdea *et al*., 2004), where the direction of convergence changed to the present WNW-ESE (Dewey *et al*., 1989; Ribeiro *et al*., 1990; Terrinha *et al*., 2003; Cunha *et al*., 2012). Since the Pliocene and Quaternary, sediment deposition has been strongly influenced by the MOW, by global climatic changes and by neotectonic activity, through reactivation of the Mesozoic NE-SW and E-W faults (Nelson *et al*., 1999; Terrinha *et al*., 2003, 2013b; Zitellini *et al*., 2004, 2009; Llave, 2006, 2019; Neves *et al*., 2009; Rosas *et al*., 2009).

2.2. Oceanographic setting

The modern oceanic circulation in the SW Portuguese Margin is driven by the interaction between several water masses at different depths (Fig. 1A). These include the North Atlantic Surface Water (NASW), the Eastern North Atlantic Central Water (ENACW), the MOW, the Labrador Sea Water (LSW), the North Atlantic Deep Water (NADW) and the Antarctic Bottom Water (AABW).

The surficial circulation is ruled by the NASW until 100 m water depth (wd) and by the southward flowing ENACW from 200 to 600 m wd, which is centered at 350 m wd with 12-16 ºC of temperature and 34.7-36.25‰ of salinity (Criado-Aldeanueva *et al*., 2006; Louarn and Morin, 2011).

The intermediate circulation is led by the MOW (Fig. 1A). The MOW originates from the Mediterranean Sea, where the constricted basin and arid climate provide the necessary conditions for the formation of warm, dense saline water, respectively, 13ºC and 36.5‰ (Ambar and Howe, 1979). The MOW forms a warm (13ºC) and dense (37‰) core, approximately 10 km wide, as it accelerates through the Strait of Gibraltar (Ambar and Howe, 1979). The MOW exits as a turbulent gravity driven flow before sinking northwest due to its high salinity and due to the interaction with seafloor irregularities (Ambar and Howe, 1979; Mulder *et al*., 2003, 2009; García *et al*., 2009; Fig. 1A). Along the South Iberian Margin, the MOW begins to raft above the NADW and deflects northward due to the Coriolis force (Zenk 1970, 1975; Baringer and Price, 1997), interacting along its pathway with the Antarctic Intermediate Water (AAIW) (Roque *et al*., 2019).

Across the SW Portuguese Margin, the MOW is composed by two main cores which flow at different depths with distinct oceanographic properties (Zenk 1970; Ambar and Howe, 1979; Ambar *et al*., 2002). The two main cores are the Mediterranean Upper Water (MU) and the Mediterranean Lower Water (ML) (Zenk 1970; Ambar and Howe 1979; Ambar *et al*., 2002, 2008). The MU is a warmer and more saline

5

water (13–14ºC and 35.7-37‰) than the ML (10.5–11.5°C and 36.5–37.5‰), flowing northward along the upper continental slope between 600 and 1000 m depth, centered at 700-800 m depth with 80-100 cm s^{-1}. The ML flows northwest between 1000 and 1400 m depth along the middle continental slope, stabilizing around 1200-1300 m wd with 20-30 cm s^{-1} (Bower *et al.,* 2002; Llave *et al.*, 2007). Underneath the MOW, the cold and fresh LSW is present between 1500 and 2200 m wd, with 3–4 ºC of temperature and 34.88‰ of salinity (Talley and McCartney, 1982).

The deep-water circulation is led by the southward flowing NADW at 2200 to 4000 m wd (Fig. 1A). The NADW was formed in the Greenland-Norwegian Sea and it is characterized as a cold (3-8ºC) and less saline (34.95–35.20‰) water mass (Reid, 1979). Underlying the NADW, the cold AABW flows northward below 4000 m wd along the Horseshoe and Tagus abyssal plains, with 2ºC of temperature and 34.76‰ of salinity (Reddy, 2001).

3. Data and Methods

The present study was carried out using a dataset of seismic reflection lines, multibeam swath bathymetry and IODP Expedition 339 drill data, available at http://iodp.tamu.edu/index.html.

3.1. Seismic reflection data

The seismic dataset used in this work consists of medium-resolution seismic reflection lines acquired in the scope of the CONDRIBER project in 2014, high-resolution seismic lines from the survey STEAM 94, low-resolution seismic lines acquired in the academic survey BIGSETS 98 and the oil-industry survey GSI 84 (Fig. 1A). The acquisition parameters of each seismic reflection survey are compiled in Table 1.

The CONDRIBER data was processed during the MOWER/CONDRIBER survey in 2014. The processing flow begun by extracting the navigation of each shot and channel through *Seisee*, followed by the calculation of the common depth point (CDP) for each seismic line and the application of a noise filter through a matlab script. The main processing flow was developed on the software *Hotshot*. Initially, the seafloor depth was digitalized in referenced bitmaps to eliminate the water column. This was followed by the equalization of the channels and shots and by high-pass filtering. Filtering was also employed through several band-pass filters, progressively applied from the seafloor down. Interference and noise from other instruments were picked up by channel 3, thus a mute was applied to remove the signal of channel 3 below 0.4 seconds. The seismic lines with sedimentary cover also underwent the elimination of the first

6

150-200 ms (below the seafloor) of channels 1 and 2, to give more emphasis to the high frequencies of channel 3. This sequence was followed by stacking of the traces by shot order, or by CDP's for the more superficial seismic reflections. This step was followed by the application of a new equalization of the traces and resampling at 1 ms. Afterwards, it was necessary to apply an Automatic Gain Control with a window of 0.7 seconds to normalize the traces. The last step was a Shift to eliminate the first 50 ms of the file and to allow synchronization between register and trigger.

The seismic reflection data was used to trace distinct seismic horizons and produce continuous surface maps for the major seismic discontinuities and total sedimentary thickness with 100 m cell size.

3.2. Bathymetric data

The bathymetry presented in this study results from two different datasets: SWIM and GEBCO (Fig. 1B). The SWIM dataset is a compilation of 19 high-resolution multibeam swath bathymetric surveys with 100 m cell size, carried out in Southwest Iberia and Northwest Morocco, covering over 180,000 km^2 from 30 m water depths closer to the shore, to 5000 m water depths in the abyssal plains (Zitellini *et al.*, 2009). The global GEBCO data, with 1852 m cell size, was remastered to 250 m cell size and used to cover the gaps left by the SWIM dataset (GEBCO, 2019).

3.3. Well data

The well data consists of stratigraphic data from Pescada-1 oil-well and lithological, downhole logging and physical properties from IODP Expedition 339 Site U1391, carried out in 2011-2012.

3.3.1. Pescada-1 oil-well data

Oil industry well Pescada-1 data was attained from other works (Matias, 2002; Batista, 2009) to correlate the older seismic horizons. The well is located southwest off Setúbal (38º08'7.1"N, 09º02'8.6"W) on the continental shelf at 148.41 m water depth and penetrated 3082.44 mbsf (meters below the seafloor) (Fig. 1A). The units and discontinuities recovered in this well comprise Mesozoic to Cenozoic deposits. The main sequences identified for this work are the Late Triassic to Early Cretaceous record at 3082.44–532.18 m depth, and the recent Neogene/Upper Miocene at 148.74–532.18 m depth (Matias, 2002).

3.3.2. Site U1391 data

7

As part of the IODP Expedition 339 from 16th November 2011 to 16th January 2012, six Sites were drilled across the Gulf of Cadiz and Southwest Portuguese Margin to research the influence of the MOW on global circulation and climate (Expedition 339 Scientists, 2012; Stow *et al.*, 2013; Hernández-Molina *et al.*, 2016b). This work uses public data from Site U1391, drilled on the Sines Drift (37º21.5322′N, 9º24.6558′W) (Fig. 1B). Three holes were drilled at Site U1391: U1391A, U1391B and U1391C. The Site penetrated 671.5 mbsf, at 1073.7 m water depth, and cored a total of 1378.1 m with a recovery of 958.57 m, which corresponds to 92.3%.

In the present work, downhole logging measurements, physical properties and visual core descriptions from Site U1391 (Expedition 339 Scientists, 2012) were downloaded from IODP's database (http://iodp.tamu.edu/index.html) and used to provide information about the lithostratigraphy, chronostratigraphy and petrophysical properties of the drilled sediments. Resistivity (ohm.m), density (g/cm^3), gamma ray radiation (gAPI), velocity (m/s), natural gamma ray (total counts cps), magnetic susceptibility (instrumental units) and color reflectance measurements a* b* L* were analyzed along with the grain size to distinguish and characterize the different seismic units and their interfaces .

4. Results

4.1. Main physiographic domains

The joint analysis of multibeam bathymetry and seismic reflection lines allowed the identification of three main physiographic domains in the Southwest Portuguese Margin (Fig. 2): the shelf, the slope (subdivided into upper, middle and lower slope) and the adjacent basin plain.

The shelf corresponds to the shallowest domain, extending from the onshore until 190 m wd with 30 km in width, over 80 km in length and 0-0.5º in dip (Fig. S1, in *supplementary material*). Submarine canyons to the north and south start from this domain, namely the São Vicente and Setúbal Canyons, and extend until the abyssal plains below 4000 m wd (Fig. 1). The transition to the upper continental slope is marked by a sharp, slightly linear shelf break at 170 to 190 m wd and is over 80 km long (Fig. 1B).

The upper continental slope develops between the shelf break and 750 m wd (Fig. 1B). The upper slope widens from south to north, characterized by a narrow, steep south slope with 5-8º in dip and 5 km in width, which gradually changes to a gentle northern slope with 1-5º in dip and 15 km in width (Fig. S1). The transition to the middle slope is marked by a steep, concave slope scarp at 750 to 1000 m wd and

by a few structural features, namely the Príncipe de Avis Seamounts in the north and the Descobridores Seamounts in the south (Fig. 1B).

The middle slope is considered the largest and most important physiographic margin domain, located between 750 and 1800 m wd and with 20 to 25 km in width (Fig. 1B). The middle slope is generally a gentle sloping surface (<1.5º in Fig. S1). The Príncipe de Avis Seamounts separate the continental slope into two sub-basins (N-S in the south and NE-SW in the north in Fig. 1B). The middle slope is characterized by the Sines Drift, its moat and few other sedimentary features (Fig. 2). The transition to the lower slope is characterized by the steep N-S Pereira de Sousa Scarp (PSS) at 1500-1800 m to 3200 wd.

The lower slope extends between 1800 and 3200 m wd, covering 50 km in length and 20 km in width (Fig. 1B) with <1.5º in dip(Fig. S1). The lower slope is subdivided into distinct depositional and erosional features, namely the Príncipe de Avis Plateau to the north, the PSS and Bow Spur to the east, and the Marquês de Pombal Plateau to the south (Fig. 2). Towards north, the transition to the basin plain is characterized by a distal slope break at 3200 m wd and marks the start of the Rincão do Lebre Basin (Fig. 1B).

4.2. Regional tectonic features

i)   Plateaus

The Príncipe de Avis and the Marquês de Pombal Plateaus define two high and extensive domains along the lower continental slope (Fig. 1B). The transition from the plateaus to the adjacent Rincão do Lebre Basin is marked by steep fault scarps at 1700 to 2800 m wd, affected by several erosional features, such as gullies, channels and head scars (Figs. 1B and 2).

The Príncipe de Avis Plateau is located between 2500 and 5000 m wd with an E-W elongated shape (Fig. 1B). The Príncipe de Avis Plateau is bounded by a steep (3-5º) angled slope along the south and forms a gentle flat surface towards north with 0-1º gradient from 2600 m wd until 5000 m wd (Fig. S1). The high relief of the plateau derives from several NE-SW buried thrust-faults.

The Marquês de Pombal Plateau is located between 1300 and 3800 m wd (Fig. 1B). This feature initially trends NE-SW before curving E-W below 2100 m wd. Along the north, the plateau forms a gentle slope with 0.5-1.5º gradient. Southward, the plateau dips towards the São Vicente Canyon with 1-5º gradient (Fig. S1). The Marquês de Pombal Plateau represents a NE-SW thrust, bound by reverse faults and an exposed fault scarp along the south (Fig. 2).

9

ii)   Basins

The Rincão do Lebre Basin is an inner basin of the Infante Dom Henrique Basin, located between 3200 and 3800 m depth and confined to the north by the Príncipe de Avis Plateau, to the south by the Marquês de Pombal Plateau and to the west by the PSS , respectively (Fig. 1B). The seafloor in the Rincão do Lebre Basin is smooth, except near the base of the PSS where it is affected by channels, gullies and mass-transport deposits (MTDs) from the nearby relief (Fig. 2).

iii)   Fault scarps

The upper slope scarp and the PSS define the most important fault-related features in the study area (Fig. 2)

The upper slope scarp defines a relatively steep and short scarp over 50 km in length, 250 m in height and 1-10º in gradient (Fig. 1B). The upper slope scarp shows a variable morphology in the south, characterized as a meandering pathway near the Descobridores Seamounts (Fig. 1B). Towards the north, the scarp trends NW-SE with 1-1.5º slopes as a gentle convex scarp (Fig. S1). Near the Príncipe de Avis Seamounts, the upper slope scarp becomes once again steep (3-10º) and bends towards the NE (Fig. S1).

The PSS marks the transition between the middle and lower slope at 1800 to 3200 m wd. The PPS is 50 km wide, 1400-200 m high and has gradients in the range of 3-15º (Fig. 1B). The PSS trends NNW-SSE to N-S, parallel to the margin. The PSS is affected by several erosional and depositional features, such as head scarps gullies and MTDs (Fig. 1B and 2).

iv)   Structural Highs

The upper slope is characterized by two high reliefs, the Príncipe de Avis Seamounts in the north and the Descobridores Seamounts in the south (Fig. 1B). The Príncipe de Avis Seamounts comprise three main structural highs at 200 to 600 m high and mark a shift in margin trend from N-S towards NE-SW (Fig. 1B). The Príncipe de Avis Seamounts represent irregular oval to NE-SW elongated reliefs, ~10 km in length, 12 km in width, and 1-10º in dip. The Descobridores Seamounts are NE-SW elongated structural highs between 200 and 300 m high (Fig. 1B). The Descobridores Seamounts are 25 km in length, 15 km in width and 3-8º in slope, approximately.

4.3. Morphosedimentary features

The Sines CDS developed along the middle and lower continental slope, which are characterized by distinct depositional and erosional features (Fig. 1B).

10

Depositional features

i)   *Plastered drift*

The Sines Drift occurs between 750 and 1800 m wd on the middle continental slope, confined by the distal segments of two submarine canyons, the Setúbal canyon to the north and the São Vicente canyon to the south (Fig. 1B and 2). Furthermore, the Sines Drift is bound in the west by the steep scarp of the Pereira de Sousa Fault (PSF) and in the east by the steeper upper slope scarp (Fig. 1B). The drift is approximately 95 km long and 35-40 km wide (Fig. 1B), covers an area over 2300 km^2 and displays an asymmetric shape with a steeper western slope (0.5-1°W in Fig. S1). The morphological features are notably different in the eastern and western sectors of the Sines Drift (Fig. S1). The eastern sector is characterized by a smooth seafloor with few sinuous sediment wave (Fig. 2) and the western sector is composed of a rough seafloor marked by several erosional features along a contourite terrace, identified as head scars, gullies and channels (Figs. 1B and 2).

ii)   *Sediment waves*

The eastern sector of the Sines Drift bears sinuous sediment waves between 800 and 1700 m wd along the middle continental slope (Figs. 1B and 2). The sediment waves possess 15-10 km long NNE-SSW crests with a low relief (<30 m; Fig. S1). In the north, the sediment waves trend parallel to the continental slope and concentrate west of the Príncipe de Avis Seamounts, while in the south and center of the slope, the sediment waves trend oblique to the continental slope and occur west of the contourite moat and northwest of the Descobridores Seamounts (Fig. 1B).

iii)   *Mass-transport deposits (MTDs)*

MTDs are mostly concentrated along the western limit of the drift (Fig. 3) and at the foot of the PSS (Fig. 1B), between 1990 and >3000 m wd within the Rincão do Lebre Basin (Fig. 1B). These deposits exhibit variable shapes and dimensions, have crests trending E-W and display convex elongated to "almond" morphologies. They are roughly 5-10 km wide, <5 km long and show ~100 m of positive relief (Fig. S1). The MTDs along the western flank of the Sines Drift occur staggered in a step-like pattern (Fig. 3) and give way to landslide scars and gullies near the PSS.

Erosional features

i)   *Submarine canyons*

The São Vicente Canyon trends NE-SW in a general direction, but it is separated into three distinct segments (Fig. 1B): the head with NE-SW from 200 to 3000 m wd, where it has several tributary

11

channels; the middle that shifts to NNE-SSW from 3000 to 4000 m wd due to a major kink of 60° at 36º50'N, 9º42'W; and the lower segment with NNE-SSW from 3000 to 4900 m wd at the abyssal plain, where the canyon has the widest bottom. The São Vicente Canyon extends over 120 km, with 200 m wd at 10 km from the shore (Fig. 1B) and 4900 m wd at the Horseshoe Abyssal Plain.

The Setúbal Canyon is characterized by a meandering shape (Fig. 1A), oriented perpendicular to the coast in an E-W direction. This canyon measures more than 100 km and reaches depths around 4900 m wd at the Tagus Abyssal Plain.

ii)   Channels

Few channels occur along the Sines CDS, mostly related to the PSS and the Bow Spur in the west (Figs. 1B and 2) or to the submarine canyons along the north and south (Fig. 1B).

The Sines Hook is a prominent channel located north of the PSS. The Sines Hook curves around the northern extent of the PSS, finally displaying a NE-SW elongation at 3200 m wd in the slope basin (Fig. 1B). The Sines Hook is marked by numerous concave scars along its northern flank and by several gullies which flow downslope in a NE-SW trend towards the deeper slope basin (Fig. 2). Its flanks vary between 3-8º in dip and extend 28 km in length (Fig. 1B).

The two channels associated with the Bow Spur form prominent erosional features, the first at 2900 m wd towards north and the second at 800 to 1400 m wd near the São Vicente Canyon (Fig. 1B). The northern channel curves towards the north and has a concave U-shaped morphology (Fig. 1B). This channel follows the same orientation as the gullies along the PSS and is roughly 1 km in wide, 8 km long and less than 100 m deep (Fig. 1B). The southern channel exhibits a slightly curving morphology and starts near a tributary branch of the São Vicente Canyon (Fig. 1B). This channel exhibits a U-shaped morphology, trending N-S before curving ENE-WSW towards the slope basin. It is 2 km wide, ~15 km long and ~200 m deep (Fig. 1B).

The channels associated with the Setúbal and São Vicente submarine canyons usually represent tributaries or feeders upslope of the canyon head and along its path (Fig. 1B). The channels are generally oriented downslope towards the canyon thalweg, oblique or orthogonal to the main canyon trend (45-90º angle). The channels are characterized by variable morphologies and dimensions, ranging between 5 and 20 km in length, 100 to 500 m in depth (Fig. 1B) and 1.5-9º in dip (Fig. S1).

iii)   Scars and gullies

12

The western sector of the Sines Drift is marked by numerous depressions between 1090 m and 2300 m depth at the head of the PSS (Fig. 1B). These features exhibit amphitheater concave shapes and head scars, which occur staggered till the lower slope (Fig. 3). These features were interpreted as landslide scars from gravity-driven events. The landslide scars give way to several V- and U-shaped gullies which incise the steep PSS with well-developed downslope E-W ridges and troughs (Fig. 1B).

iv)   Moat

The Sines Drift has an eastern moat, ~80 km long, 0.5-1 km wide and 50 m deep (Fig. S1), located between 750-1400 m wd with NNW-SSE to NNE-SSW orientation (Fig. 1B). The moat starts at the south, near a branch of the São Vicente Canyon, and follows the upper continental slope towards the Setúbal Canyon (Fig. 2). The moat exhibits a V-shaped morphology in the south, which gradually transitions into a U-shaped morphology in the center of the study area. To the west of the Príncipe de Avis Seamounts, the moat narrows to a V-shaped feature with lower incision depths (<100 m deep and <0.5 km wide; Fig. 1B).

Mixed features

iv)   Terrace

The western to central sector of the Sines Drift is characterized by a contourite terrace between ~1300 and 1800 m wd (Fig. 1B). The contourite terrace corresponds to a smooth, flat (0.5-1°) surface, that is >50 km in length and 10-15 km in width (Figs. 1B and S1). In general, the terrace is wider in the south at 1300 to 1800 m wd and narrows northward, where it is located between 1700 and 1900 m wd (Fig. 1B).

4.4. Seismic stratigraphy

Six seismic units have been identified in the Sines CDS (from older to younger, U6 to U1), bounded by seismic horizons B to H1 (Figs. 3 to 8). The contourite sedimentary succession lies over an important basal discontinuity, named the B unconformity (Figs. 3 to 6). The B unconformity represents a very high amplitude reflection with a highly visible and laterally continuous erosional surface (Fig. 4). This unconformity truncates older Paleogene to Late Cretaceous deposits, characterized by high to low amplitude irregular or deformed reflections (Fig. 5). Along the shelf, the B unconformity highlights the prominent relief of the ENE-WSW Príncipe de Avis Seamounts and the paleo-relief created by distinct, buried tectonic structures, such as grabens and horsts (Fig. 9B). The Sines Drift is deposited between two major structural highs: the western horst **h1** and the eastern horst **h2**. (Fig. 3). Horst **h1** is limited by fault

13

F1 to the east and by the PSF to the west, which marks the transition from the middle to the lower slope through the exposed PSS (Fig. 1B). The PSF is a normal fault that can be subdivided into two segments due to a shift in orientation from N-S towards NNE-SSW (Fig. 1B). F1 is a normal NNW-SSE trending fault with 40 km length (Fig. 9). Horst **h2** is bounded by fault F2 in the west and by a minor normal fault in the upper continental slope towards the east (Fig. 4). Fault F2 has NNW-SSE orientation which changes to NNE-SSW towards the north, with 75 km of extension (Fig. 9B). F2 also marks the transition between the upper and the middle continental slope through an exposed slope scarp (Fig. 2). East of horst **h1**, faults F1 and F2 limit a central graben **g1** (with NNW-SSE to N-S elongation) within the middle continental slope (Fig. 9B). The Sines CDS was deposited over this graben and towards the north of the study area (Fig. 9A).

The distribution of the seismic units above the B unconformity highlight a variable sedimentary distribution with three main depocenters: D1 in the south, D2 in the center and D3 in the north (Fig. 9A). D1 and D2 are confined by horsts **h1** and **h2** to the east and west, and D3 is confined by horst **h2** to the east and unconfined towards the Príncipe de Avis Plateau (Fig. 9A). Furthermore, D1 strikes NE-SW in an oblique direction to the margin trend, while D2 elongates N-S parallel to the margin and D3 strikes NE-SW, parallel to the northern margin trend (Fig. 9B).

The oldest seismic unit identified is unit U6, which lies over the B unconformity and is topped by horizon H5 (Fig. 3). Seismic unit U6 is characterized by parallel low amplitude and continuous reflections onlaping towards the south. It has semi-transparent facies and displays a sheet shape (Fig. 5), with an average thickness of 200 ms TWT and a maximum thickness of 530 ms TWT (Fig. 3). U6 can be sub-divided into two sub-units U6B and U6A. U6B is characterized by high to low amplitude reflections in a wedge configuration, which gradually changes to low amplitude to semi-transparent reflections with sheeted configuration in U6A (Fig. 6). U6 is thicker in the southern and center depocenters (D1 and D2) as an aggradational sheet that thickens towards the west and covers horst **h1** (Fig. 3).

Seismic unit U5 is bounded at the base by horizon H5 and at the top by horizon H4 (Fig. 5). H5 exhibits moderate amplitude and good lateral continuity, marked by toplap terminations of U6 (Fig. 3). Seismic unit U5 shows a similar facies and configuration as seismic unit U6, with low amplitude, continuous and subparallel reflections and divergent reflections when it encounters structural highs at the boundaries of the basin (Fig. 6). Unit U5 is a thick and widespread unit, with sheet configuration and average thickness of 220 ms TWT (maximum thickness of 250 ms TWT) (Fig. 3). Along the middle

14

slope, U5 continues to fill the main depocenters D1 to D3 (Fig. 3). The deposition of U5 is also characterized by the development of paleochannels west of the central depocenter (D2) around seafloor irregularities, mostly structural features associated with horst **h1** (Fig. 6).

Seismic unit U4 lies on top of horizon H4 and is topped by horizon H3 (Fig. 3). Horizon H4 is a moderate amplitude reflection, laterally continuous and marked by toplap terminations of U5 (Fig. 6). Seismic unit U4 shows variable low to medium amplitude, parallel reflections with good lateral continuity and semi-transparent facies (Fig. 6). The distribution of unit U4 is again widespread, in a sheet configuration, with an average thickness of 130 ms TWT and maximum thickness of 150 ms TWT (Fig. 6). The distribution of U4 resembles that of U5, with less sedimentary thickness along the continental slope (Fig. 3). U4 shows thicker deposition in the south and center depocenters (D1 and D2) near horst **h1**, resembling the wedge to sheeted configuration of U6A (Fig. 3).

Seismic unit U3 is bounded by horizon H3 at the base and horizon H2 at the top (Fig. 6). Horizon H3 is a high amplitude and laterally continuous reflection, marked by toplap and truncation reflections of the underlying units (U4 to U6), denoting, respectively, its non-depositional and erosive character (Fig. 4). Horizon H3 shows a gradual shelf, marked by a smooth transition to the middle slope and a less defined relief of the Príncipe de Avis Seamounts (Fig. 9C). The middle slope is still marked by faint depressions along graben **g1**, however the margin shows a smoother and more gentle slope. The transition to the lower slope in H3 is more gradual and indicates the burial of horst **h1** (Fig. 9C). Seismic unit U3 is characterized by a significant change in acoustic facies, with stratified facies and moderate to high amplitude, parallel, laterally continuous reflections (Fig. 6). This unit is also characterized by chaotic and irregular reflections in the southeast, indicating multiple internal erosional surfaces. They are related to the erosion and infill of channel features, interpreted as paleomoats (Fig. 4). This unit reaches an average thickness of 110 ms TWT and maximum thickness of 280 ms TWT with a sheeted configuration (Fig. 3) that changes laterally, in the southeast and near the Príncipe de Avis Seamounts, into a mounded, progradational, sigmoid-oblique configuration (Fig. 4). U3 is further characterized by the upslope infill and progradation of the paleomoats, with considerable dimensions in the northern depocenter D3 and associated to the formation of sediment waves of variable dimensions (Fig. 4).

Seismic unit U2 is bounded by horizon H2 at the base and horizon H1 at the top (Fig. 4). Horizon H2 is a moderate to high amplitude reflection with good lateral continuity, marked by toplap terminations of U3 internal reflections and downlap terminations of U2 reflections (Fig. 6). In places, H2 is conformable

15

with the subsequently deposited unit, namely U2 (Fig. 4). Unit U2 has stratified facies with high amplitude and continuous reflections in the center of the basin, which change to irregular reflections in the southeast, related to the fill of a paleomoat (Fig. 4). This unit has an average thickness of 190 ms TWT and maximum thickness of 330 ms TWT with a sheeted configuration (Fig. 3) that changes to a mounded to sigmoid-oblique configuration in the south and in the north, near the Príncipe de Avis Seamounts (Fig. 4). The deposition of U2 resembles that of U3, with infill of paleomoats (progradational pattern) along the south to northern depocenters (Fig. 6). In the north, U2 is heavily eroded, despite still prograding upslope and forming significant paleomoats and sediment waves (Fig. 4).

The most recent seismic unit is U1 bounded by horizon H1 at the base and by the seafloor at the top (horizon S; Fig. 3). Horizon H1 is a high amplitude, continuous and parallel reflection, marked by toplap terminations of unit U2 (Fig. 4). Unit U1 is defined as a widespread unit with stratified facies characterized by parallel and high amplitude internal reflections, defining a sheet configuration (Fig. 6). Locally, sediment waves are observed within and on top of U1. Unit U1 reaches a maximum thickness of 340 ms TWT with an average of 280 ms TWT. U1 is characterized by the incision of small paleomoats in the east (70-40 m wide and 50-20 m deep), marked by toplap terminations of the underlying sub-units and low to high amplitude reflections (Fig. 6). Seismic unit U1 shows an aggradational configuration (Fig. 6). U1 marks a change in deposition, with the formation of significant sediment waves in the northern depocenter D3 (Fig. 4). In the southern and central depocenters (D1 and D2), U1 shows a uniform, draping deposition (Figs. 3 and 6). Seismic unit U1 can be divided into three sub-units (from bottom to top, U1C, U1B and U1A) separated by two internal discontinuities, horizons H1$_B$ and H1$_A$, both marked by toplap terminations on the underlying sub-units and downlap terminations on the overlying sub-units (Fig. 4). These discontinuities represent erosional unconformities on the basin margins, close to the flanks of structural highs, changing laterally to concordance in the middle of the basins (Fig. 6). Furthermore, the surface of horizon H1$_B$ shows a gentle transition from the shelf towards the middle slope and lower slope, indicating the previous paleo-reliefs have been gradually buried (Fig. 9D).

4.5. Lithology and physical properties of seismic units

The lithology and petrophysical properties of the seismic units were studied through Site U1391 data (Fig. 10). Seismic unit U5 (632-671.5 mbsf) is dominated by calcareous mud, interbedded with medium to thick calcareous silty mud beds from 637.1 to 640.8 mbsf, with subtle parallel laminae occurring

16

locally (Fig. 10). These lithologies characterize very rare and thin contourite sequences, which coarsen from calcareous mud to calcareous silty mud and then to calcareous mud with gradational contacts. This unit also has silty mud with biogenic carbonate (with biosiliceous and carbonate fossils) at 650.1-652.1 mbsf (Fig. 10).

The transition to seismic unit U4 (566-632 mbsf) is marked by a dolomite mudstone of ~0.87 m at 632 mbsf (Fig. 11C), which is identified by high resistivity (2.8 ohm.m), density (2.6 g/cm^3), velocity (2.9 km/s), magnetic susceptibility (20 inst. units), color reflectance measurements (a* b* L*) and low NGR (22 cps) (Fig. 10).

Seismic unit U4 is characterized by calcareous mud interbedded with thick beds of calcareous silty mud that correspond to thin rare contourite sequences (with foraminifers and biosiliceous fossils, such as sponge spicules). This unit also has mud with biogenic carbonate (with biosiliceous fossils) of 0.20 m above the dolomite mudstone and a debrite of 0.35 m at 604 mbsf with muddy intraclasts and matrix (Fig. 11B). Seismic units U5 and U4 have clearly recognized low values for all physical properties: resistivity (1.5-2 ohm.m), density (1.6-1.9 g/cm^3), gamma ray (30-50 gAPI), velocity (2-2.2 km/s), NGR (30-42 cps), magnetic susceptibility (10 inst. units) and color reflectance L* (Fig. 10), as well as a positive correlation between resistivity, density and gamma ray (Fig. 10). The transition to seismic unit U3 is marked by an increase of resistivity (1.5-2 ohm.m), density (1.6-2.1 g/cm^3), gamma ray (30-60 gAPI), velocity (2-2.2 km/s), NGR (30-50 cps) and magnetic susceptibility (10 inst. units) (Fig. 10).

Seismic unit U3 (400-566 mbsf) is dominated by calcareous mud interbedded with calcareous silty mud beds. These lithologies characterize rare contourite sequences, coarsening-up from calcareous mud to calcareous silty mud, then fining-up to calcareous mud with gradational contacts and no coarse grain size sediments. This unit also has very low angle cross lamina at 461.1 mbsf with 0.3 m and a diatom rich biogenic mud bed at 525.6-526.3 mbsf (Fig. 10). Seismic unit U3 displays a positive correlation with higher values of resistivity (1.6-2.1 ohm.m), density (1.5-2.2 g/cm^3), gamma ray (25-60 gAPI) and NGR (30-50 cps) (Fig. 10). The transition to seismic unit U2 is marked by lower values of density (1.6 g/cm^3) and velocity (1.7 km/s) (Fig. 10).

Seismic unit U2 (196-400 mbsf) is dominated by calcareous mud, interbedded with silty mud with biogenic carbonate and with calcareous silty mud beds (Fig. 10). These lithologies characterize contourite sequences with bigradational and normal grading. This unit also has small concentrations of quartz occurring locally and nannofossil mud and biosiliceous mud at 253.3-254.3 mbsf. Seismic unit U2 shows

17

a positive correlation between density and gamma ray, as well as a high scatter of data with lower values of resistivity (1.1-2.1 ohm.m), density (1.1-2 g/cm^3) and velocity (1.6-2 km/s) (Fig. 10). The transition to seismic unit U1 is marked by a calcareous sandy mud bed of ~1.2 m with lower values of density (1.4 ohm.m), gamma ray (25 gAPI) and velocity (1.7 km/s) and higher values of magnetic susceptibility (17 inst. units) and color reflectance L* (45) (Fig. 10).

Seismic unit U1 (0-196 mbsf) is dominated by calcareous mud from 42.1 to 196 mbsf and by mud with biogenic carbonate from the seafloor to 42.1 mbsf. This unit has a high number of calcareous silty mud, calcareous sandy mud and calcareous silty sand beds. These lithologies are associated with several bigradational contourite successions with gradational contacts, which coarsen-up from calcareous mud to calcareous silty mud and calcareous silty sand, then fining-up to calcareous silty mud and calcareous mud (Fig. 11A). Sharp basal contacts or rarer erosional contacts also occur and cut the contourite successions and therefore partial bigradational, normal or reverse grading are also common. Unit U1 is separated into three sub-units in the seismic record, U1C, U1B and U1A, which is also observed in the sedimentary record due to facies variation (Fig. 10).

Seismic sub-unit U1C (96-196 mbsf) is characterized by calcareous mud, with a large range of bigradational contourite successions (Fig. 11A) which coarsen-up from calcareous silty mud to a maximum grain size of sandy mud or silty sand and then fine-up to calcareous silty mud (with abundant diatoms and sponge spicules at 91.6-22.6 mbsf). This unit also has interbedded nannofossil mud at 89.6-91.6 mbsf. Seismic unit U1C displays low values of density (1.5-2 g/cm^3), gamma ray (40-60 gAPI) and velocity (1.6-1.7 km/s) and a large scatter of data for resistivity (0.8-2.5 ohm.m) and color reflectance (b* with values of 30-50) (Fig. 10). Seismic sub-unit U1B (42.1-96 mbsf) is dominated by calcareous mud, alternating with mud with biogenic carbonate. This unit consists of several bigradational sequences, coarsening-up from calcareous mud to calcareous silty mud and sandy mud, then fining-up to calcareous silty mud and calcareous mud (Fig. 11A). In contrast, seismic sub-unit U1A (0-42.1 mbsf) is dominated by mud with biogenic carbonate, with minor presence of silty or sandy mud beds with biogenic carbonate. These alternations also correspond to bigradational contourite successions. Some bigradational successions have sharp to erosional contacts in the middle of the succession, which is at the base or top of the successions with maximum grain size (Fig. 10). Local occurrence of shell fragments of pteropods and rare gastropods at 4.1-13.85 mbsf and rare scaphlopoda at 13.6-23.32 mbsf. Seismic sub-units U1B and

18

U1A (0-96 mbsf) show a positive correlation between NGR, magnetic susceptibility and color reflectance measurement L* (Fig. 10).

5. Seismic Interpretation

5.1. Chronostratigraphic constraints for seismic discontinuities and units

The ages of the seismic units and the seismic discontinuities was constrained through well Pescada-1 and Site U1391 data. The seismostratigraphic correlation is presented in Figs. 7 and 8.

Pescada-1 well correlated the B unconformity, the lower boundary of the Sines CDS, to the Late Miocene (Fig. 7). The deposits beneath the B unconformity correspond to Early Cretaceous deposits on the continental shelf (Fig. 7), however, Late Cretaceous to Paleogene deposits were inferred to exist on the continental slope since the stratigraphic strata is considerably thicker (Fig. 7). The true age of the B unconformity on the continental slope is unknown, but seismic unit U6 which was deposited after the B unconformity, was inferred as Late Miocene deposits (Fig. 7 and Table 2).

The age for the base of unit U5, marked by seismic horizon H5, has not been drilled by wells, however further stratigraphic information was secured by cross-referencing our units and horizons with the seismic units and discontinuities described in previous studies (Table 2). Horizon H5 was correlated to the M discontinuity (at 5.33 Ma), which allowed us to assign an Early Pliocene age to seismic unit U5 (Table 2).

Site U1391 data (Expedition 339 Scientists, 2012) allowed a correlation between the main lithostratigraphic units and discontinuities and the seismic units and discontinuities recognized in the Sines Drift (Figs. 5 and 8). The bottom of U1391C borehole at 671.5 mbsf reached Late Pliocene sediments (estimated to span 3.31-3.5 Ma) below seismic horizon H4, which corresponds to the top of seismic unit U5 (Fig. 8). Hence, a Late Pliocene age was assigned to the uppermost part of seismic unit U5 deposits. This also allowed to assign a Late Pliocene (Piacenzian) to Early Quaternary (Gelasian) age to seismic unit U4, since horizon H4 corresponds to the *Late Pliocene Discontinuity* (*LPD*) at 3-3.2 Ma. Seismic unit U3 was assigned an Early Quaternary (Gelasian), since horizon H3 correlates to the *Early Quaternary Discontinuity* (*EQD*) at 2.5-2.4 Ma. An Early Quaternary (Calabrian) age was assigned to seismic unit U2, where seismic horizon H2 was inferred as the base of the Calabrian. A Middle Pleistocene to Holocene age was assigned to seismic unit U1, since horizon H1 corresponds to the *Middle Pleistocene Discontinuity* (*MPD*) at 0.7-0.78 Ma, horizon H1$_B$ corresponds to the *Late Quaternary*

19

Discontinuity (*LQD*) at 0.4 Ma and Horizon H1$_A$ was estimated at 15.6-20 ka. (Expedition 339 Scientists, 2012; Hernández-Molina *et al*., 2016b; Fig. 8 and Table 2).

Site U1391 data also estimated sedimentation rates for certain intervals, with 13 cm/ky during the Pliocene, 17cm/ky from 2.58-1.5 Ma in the Pleistocene and 27 cm/ky from ~1.5 Ma to the present-day seafloor (Expedition 339 Scientists, 2012).

5.2. *Sedimentary stacking patterns*

The distribution and internal configuration of the seismic units highlight a variable stacking pattern and sedimentary architecture from the Late Miocene to the Quaternary. The distribution of U6 (Latest Miocene – 5.3 Ma) and its basal unconformity B follows the three main depocenters: D1 in the south, D2 in the center and D3 in the north (Fig. S2A). The deposition of U6 mostly fills the southern and central depocenters (D1 and D2), where it thickens outwards over horst h1 with 200-530 ms in thickness (Fig. S2A). In the western part of the study area, deposition during U6 is marked by westward downslope processes near the PSS (Fig. 6), evidenced by interbedded semi-transparent to chaotic packages within U6, indicating frequent MTDs towards the middle of the depocenters. Furthermore, the deposition of U6B mostly covers the seafloor irregularities produced during H6$_A$, while U16A homogenizes over the entire margin (Fig. 3).

The distribution of U5 (5.3 – 3.2 Ma) is overall thinner compared to U6 (~220 ms on average), however it has a more uniform distribution over the entire margin (Fig. 6). During U5, deposition continue to fill the main depocenters and homogenizes the margin morphology. Nevertheless, thinner deposits are present near horst h2 (~100 ms) due to the development of erosive N-S paleochannels around paleo-reliefs (Fig. 6). Towards the west, U5 is characterized by less sedimentary thickness (50-100 ms) over horst **h1** and near the steep PSS due to active downslope gravity-driven processes (Fig. 5). The paleochannels also appear to have been filled by low amplitude chaotic packages, characteristic of MTDs (Fig. 6). These deposits were probably generated by sediment overspill from the nearby upper slope and were trapped within the paleochannels (Fig. 6). Furthermore, their alongslope elongation towards north indicates active reworking by bottom-currents (Fig. S2A).

The distribution of U4 (3.2 – 2.5 Ma) resembles that of U5, albeit thinner (130 ms on average) over horst **h1** as a result of non-deposition, or most likely active gravity-driven processes towards west (Fig. 3). U4 also fills the paleochannels produced during U5, however their high amplitude seismic pattern

20

indicates draping rather than MTD-infill (Fig. 6). In the northern depocenter (D3), U4 thins towards the east due to subsequent erosion produced during H3 (Fig. 4). The sedimentary stacking pattern of U4 to U6 defines the formation of a sheeted plastered drift. The gradual deposition of the sheeted drift, draping over the previous structural highs and seafloor irregularities (Fig. 9B), gentled the overall margin trend (Fig. S2A).

U3 (2.5 – 1.5 Ma) records an important change in the sedimentary stacking pattern. This change is marked by significant erosion of the previous units and the establishment of large paleomoats along the entire margin (Fig. 6). Furthermore, U3 shows clear aggradational stacking patterns, smoothing the overall margin morphology (Fig. S2B). In the northern depocenter D3, U3 is thinner (110 ms on average) due to the subsequent erosion (marked by H2) and the formation of upslope prograding sediment waves during U2 (Fig. 4).

The deposition of U2 (1.5 – 0.7 Ma) is similar to U3, marked by infill and progradation of the eastern paleomoats along the southern and northern depocenters (Fig. 6). However, U2 is thicker than U3 along the entire margin (190 ms on average) and displays a more sheet-like configuration which thins towards the west and is elongated parallel to the margin (Fig. 3). The subsequent erosion and formation of sediment waves during U1 partially eroded the top of seismic unit U2 along the northern depocenter D3 (Fig. 4). The sedimentary stacking patterns of U2 and U3 characterize a change from sheeted plastered drift towards a thick mounded plastered drift (Fig. S2B), with significant palemoats along the east, concentrated along the scarp of horst **h2** (Fig. 6). These paleomoats indicate a northward flowing bottom-current, locally enhanced by the structural constraints (horst **h2**).

U1 (0.7 Ma – present) deposition begins with a shift in margin morphology, due to the formation of variable sediment waves in the north (Fig. 4). The sediment waves show a significant upslope migration, resulting in a decreasing thickness of the unit from the continental slope towards the west (~350 to 200 ms thickness on average). In the southern and central depocenters (D1 and D2), U1 has a fairly uniform thickness marked by active mass-transport processes in the west and by small variations between U1C, U1B and U1A in the east (Figs. 3 and 6). U1C is characterized by a slight concave morphology near horst **h2**, due to an undefined paleomoat along the east, and higher thickness within the depressions produced during U2 (e.g. within the previous paleomoats and downward of sediment waves; Fig. 4). Overall, U1C shows a uniform and tabular deposition within the southern and central depocenters, D1 and D2. U1B resembles U1C within D1, however it shifts towards a mounded morphology as it fills the eastern

21

paleomoat along D2 and D3 (Fig. 6). Within depocenters D2 and D3, U1B forms a thin lenticular to sheeted shape thinning towards west. The last subunit U1A resembles U1C as a uniform and tabular appearance within D1 and D2. However, U1A has higher thickness and shows more aggradation than the previous subunits and appears to smoothen the previous morphology (Figs. 9D and 6). In general, the stacking pattern of U1 indicates a gradual transition from mounded plastered drift towards a more tabular plastered drift (Fig. S2B). This change is associated cyclic stacking patterns of alternating low to high amplitude reflections (Fig. 3) and a gentle alongslope morphology (Fig. 6).

6. Discussion

6.1. Influence of tectonics on the formation of the Sines Contourite Depositional System

The Late Miocene to Holocene contourite succession is deposited between two major structurally controlled basement highs: the western horst **h1** and the eastern horst **h2** (Fig. 9A). The horst **h1**, bounded by PSF and F1, controlled the deposition of seismic units U0 through U1 (Late Miocene to Holocene deposits) reducing the accommodation space available for the Sines Drift development. Therefore, this drift is thinner above the horst (Fig. 5). Horst **h2** completely blocks the development of the Sines CDS towards east, acting as a barrier (Fig. 3). East of horst **h1**, faults F1 and F2 limit graben **g1** in the center of the continental slope, which provided the accommodation space needed for drift deposition (Fig. 3) while horsts **h1** and **h2** did not allow a lateral migration of the drift and instead permitted a more vertical growth (Fig. 9A). Furthermore, the presence of several (paleo)moats in the east along the middle continental slope (Fig. 3) reveals that the pathway of the MOW is probably constrained by this paleomorphology (Fig. 9B). The horsts acted as lateral barriers to the MOW current, which flowed northwards along the continental slope as a geostrophic contour-current, being pushing right by the Coriolis force.

The horsts and grabens are structures inherited from the Mesozoic rifting processes on the Southwest Iberian Margin, which divided the margin into multiple segments (Alves *et al*., 2002, 2006, 2009, 2013; Pereira and Alves, 2010, 2011; Ribeiro, 2013; Terrinha *et al*., 2013a, 2013b; Fig. 9B). The N-S trending faults PSF, F1 and F2 acted as extensional faults during the Mesozoic rifting and were not reactivated as reverse faults during the tectonic inversion in the Cenozoic since the sediments on their hanging walls do not show any signs of compression (Fig. 3). The PSF is dissected by NE-SW reverse faults to the north and south (Fig. 9B), suggesting a NW-SE compression direction, consistent with the orientation of the Alpine tectonic inversion. Those NE-SW reverse faults define fold and thrust structures (Fig. 9B) from

22

the Príncipe de Avis Seamounts in the north and from the Marquês de Pombal Plateau in the south (Figs. 1B and 14). The NE-SW reverse faults are rooted in the Mesozoic extensional faults, which were inverted during the Miocene tectonic inversion related to the Betic orogeny. Therefore, while the sediments of the Sines Drift are notaffected by the major tectonic shifts (Fig. 6), the effects of the tectonic inversion are being accommodated by reverse faults and the middle continental slope is probably experiencing uplift (Fig. 5). Onshore neighboring areas have recorded an uplift rate of 0.1-0.2 mm/yr since the Late Pleistocene (Figueiredo *et al*., 2013), which could extend further offshore until the continental slope. The numerous landslide scars and gullies along the foot of the PSS suggest decreased sediment accommodation and oversteepening, associated with the ongoing uplift and other preconditioning factors (Neves *et al*., 2016; Teixeira *et al*., 2019).

6.2. Decoding the paleoceanography of the MOW

The existence of lithological variations throughout the sedimentary record and in the Sines Drift's sedimentary stacking pattern indicates that different processes influenced the development of the drift. Therefore, we can infer that during the deposition of seismic units U4 to U6 in the Latest Miocene to Late Pliocene, the MOW flowed as a weak bottom-current and secondary processes occurred intersected. The sediments of seismic units U4 and U5 are characterized by rare bigradational contourite sequences, as well as mud with biogenic carbonate, a dolomite mudstone and a debrite (Figs. 10, 11B and 11C), suggesting a mixed system marked by the occurrence of other depositional processes (such as downslope and upwelling events) during the formation of a sheeted drift by a weak MOW. A similar mixed system has been identified south of the Algarve margin (Llave *et al*., 2007, 2011; Roque *et al*., 2012; Brackenridge *et al*., 2013) and along the Galician and Ortegal drifts across the North Iberian Margin (Ercilla *et al*., 2011; Llave *et al*., 2019).

In the Late Pliocene to Early Quaternary (U2 and U3), the Sines Drift changes towards a mounded drift with moat-formation and alternating high to low amplitude seismic packages (Figs. 3 and 6), suggesting the shift was triggered by the formation of a denser and more intense MOW. According to Hernández-Molina *et al*. (2016b), the period between the *LPD* and *EQD*, which correspond to seismic horizons H4 and H3 (3.2-2.4 Ma), marks a major enhancement and vigorous circulation of the MOW (Fig. 12). Other contourite systems around the Iberian and Cantabrian Margins share similar responses

23

with the formation of mounded drifts and deep moats (Hernández-Molina *et al*. 2016b; Llave et al., 2019; Liu *et al*., 2020).

The Quaternary is characterized by the development of a plastered drift since 0.7 Ma (seismic unit U1), with alternating erosional and depositional contourite features (moats and sediment waves; Fig. 4). These features are frequently associated with alternating high to low amplitude seismic packages (Fig. 3) and muddy-sandy contourite successions at Site U1391 (Fig. 10). These changes are associated with two important hiatuses in the Middle Pleistocene: the *Middle Pleistocene Revolution* (*MPR*, 0.7-0.78 Ma) and the *LQD* (~0.4 Ma) (Miller *et al*., 2005; Llave *et al*., 2007; Lofi *et al*., 2016). Seismic data shows that the *MPR* (seismic horizon H1) is associated with high amplitude stratified facies and minor erosive surfaces (Fig. 4). The *LQD* is marked by seismic horizon $H1_B$ and is characterized by a small paleomoat and by a high amplitude basal reflection (Fig. 6). At Site U1391, the *MPR* and *LQD* coincide with an increase in coarse-grained sediments and bigradational contourite successions (Fig. 11A). These changes suggest two periods of MOW enhancement (Fig. 12).

However, another important change occurs during the Quaternary, which is marked by horizon $H1_A$ at 20-15.6 ka (Fig. 12). This period is characterized by the development of the present moat with high amplitude internal reflections (Fig. 3) and by the common occurrence of bigradational contourite successions in the lithological record (Fig. 11A). Since the moat and the sedimentary stacking pattern retain the same configuration until the present seafloor, horizon H_{1A} at 20 ka probably marks an enhancement of the MOW before shifting towards the present circulation pattern. A recent study on the Upper Quaternary record has shown that an enhancement of the MOW at ~30.5-17.1 ka is responsible for an increase of the terrigenous input at the facies scale (Teixeira *et al*. 2020). Therefore, the changes seen at a seismic and facies scale have been interpreted as a result of major long-term variations of bottom-current intensity and depth (Fig. 12).

The variations in morphology, stacking pattern and thickness of the Sines Drift suggests that the largest contourite accumulation occurred during times of glacio-eustatic lowstand with a vigorous deep and dense MOW flowing along the margin (Fig. 12). Several seismic works and proxy studies have described a denser and enhanced MOW during glacial times, flowing 700 m deeper than today (the MOW's main core flows at ~800 m depth in the Present and flowed at 1600-2200 m depth in the past) (Cacho *et al*., 2000, 2002; Schönfeld and Zahn, 2000; Rogerson *et al*., 2005, 2012; Voelker *et al*., 2006, 2015; Toucanne *et al*., 2007; García *et al*., 2009; Hernández-Molina *et al*., 2014; Teixeira *et al.* 2020).

24

High-resolution studies also suggest that the enhancement of the MOW probably occurred during Heinrich events, Dansgaard-Oeschger stadials and Younger Dryas (Sierro *et al*., 2005, Llave *et al*., 2006, Voelker *et al*., 2006, 2015). During glacial-interglacial transitions, variabilities of the thermohaline circulation, the Atlantic inflow signal and of the local run-off resulted in short-lived intensifications of the MOW's upper branch, between 600-1000 m water depth, while the MOW's lower branch decreased in strength and retreated to shallower depths (Cacho *et al.*, 2002, 2006; Schönfeld and Zahn, 2000). By contrast, during the interglacials a weaker and less dense MOW allowed for oxygenation of deep-water masses and better preservation of biogenic content (Cacho, 2000; Voelker *et al*., 2006, 2015; Toucanne *et al*., 2007). The present circulation pattern of the MOW was established after the Younger Dryas, between 7.5 and 5.5 ka (Rogerson *et al*., 2005, 2006; García *et al*., 2009).

6.3. Evolution of Sines drift deposition

Through seismic stratigraphy interpretation and mapping of the seismic units, three main stages of contourite sedimentation have been identified, characterized by different morphologies and stacking patterns (Fig. 13): 1) *onset and initial stage*, 2) *growing stage* and 3) *maintenance stage*.

1. Onset and initial stage (Late Miocene to Late Pliocene, 5.33 – 2.5 Ma)

The initial stage, represented by seismic units U4 to U6, was interpreted as a preliminary phase of contourite formation (Fig. 13) where a sheeted drift was restricted by paleo-reliefs (horsts **h1** and **h2**; Fig. 9A and 9B). This stage occurred from the Late Miocene until the Late Pliocene, after an erosional event during the Tortonian (seismic horizon B; Fig. 5). This was an erosive episode which changed the seafloor morphology of the Alentejo Margin. Although the precise age of this event remains unknown, it could be linked to regional tectonic and paleoceanographic changes that took place during the end of Late Miocene (Hsü *et al*., 1973; Sierro *et al*., 2008; Flecker *et al*., 2015; Capella *et al*., 2018). Among them are the closure and opening of the Mediterranean and Atlantic gateways (Flecker *et al*., 2015; Capella *et al*., 2018, 2019). However seismic unit U6 consists of older deposits (<5.33 Ma), buried below the modern contourite system, built since the Pliocene until the present (U5 to U1) (Fig. 12). Therefore, these ancient features need to be studied in further detail to establish their relations with the regional tectonic and paleoceanographic changes. During the initial stage, U6 to U4 are dominated by the formation a sheeted drift with a non-erosive contourite terrace (Fig. 3) and low sedimentation rates of 13 cm/ky during the

25

Pliocene (Expedition 339 Scientists, 2012), suggesting the presence of a weak bottom-current. The recovery at site U1391 of mixed facies with mud rich contourites, mud with biogenic carbonate, dolomite mudstone and debrite for U4 and U5 (Fig. 10) characterizes a more complex depositional environment, not entirely dominated by alongslope processes (Fig. 12). Other processes occurred during Stage 1, such as downslope events, which are corroborated by the debrite of ~35 cm thickness with muddy intraclasts and matrix (Fig. 11B). The resolution of the seismic data might obscure the identification of these relatively small downslope sedimentary features. However, MTDs and paleo-MTDs are present throughout the seismic record on the western sector of the Sines Drift (affecting U1 to U6 in Fig. 5). Other works in the study area have mapped these significant downslope mass-transport processes and found them to be mostly associated with the steep PSS or other slope scarp (Neves *et al*., 2016; Teixeira *et al*., 2019) and the nearby submarine canyons (Serra *et al*., 2010). Recently, Mencaroni *et al*. (2020) identified a mixed system across the Marquês de Pombal Plateau, near the São Vicente Canyon, formed by the interaction between downslope and alongslope processes. Similar mixed systems have been identified during the Pliocene along the Gulf of Cadiz, Galicia, Ortegal and Le Danois CDS, where alongslope and downslope interaction led to alternations of contourite and gravity-driven deposits (Llave *et al*., 2007, 2011, 2018; Roque *et al*., 2012; Brackenbridge *et al*., 2013; Ercilla *et al*., 2011; Hernández-Molina *et al*., 2006; Liu *et al*., 2019, 2020). Contourite systems across other continental margins report a similar sediment build-up under weak bottom-current conditions (Van Rooij *et al*., 2007; Juan *et al*., 2016, 2020; Miramontes *et al*., 2016). Therefore, the initial stage of this system is marked by an initially weak paleo-MOW, which probably flowed as a single core along the continental margin (Stow *et al*., 2013; Hernández-Molina *et al*. 2014) and led to the formation of a sheeted drift intercalated by other sedimentary deposits. Several works show that humid climate conditions prevailed in the Mediterranean until 3.4 Ma (Béthoux and Pierre, 1999), inducing the occurrence of a weak flowing MOW, until the climate changed later in the Late Pliocene to cold and arid. The rise in the Mediterranean summer aridity occurred between the *LPD* and the *LQD* (at 3.2 to 2.4 Ma) which triggered production of cooler, saltier and denser Mediterranean deep water (Hayward *et al*., 2009; Khélifi *et al*., 2009; Fig. 12). The MOW would therefore have an enhanced deep-water convection within the Mediterranean Sea, which led to a vigorous outflow and enhanced activity along the Iberian continental margin (Khélifi *et al*., 2009, 2014; Hernandez-Molina *et al*., 2014).

2. Growing stage (Early to Middle Pleistocene, 2.5 – 0.7 Ma)

The second evolutionary stage is characterized by the development of a mounded contourite drift which is constituted by seismic units U2 and U3 (Fig. 13). A significant transition occurs, from sheeted drift to mounded drift (Fig. 13), marked by a discontinuity (seismic horizon H3) and by small upslope migration and incision of prominent paleomoats (Fig. 4). Site U1391 data estimated average to high sedimentation rates for the Pleistocene with 17 cm/ky from 2.58 to 1.5 Ma and 27 cm/ky since ~1.5 Ma (Expedition 339 Scientists, 2012). Furthermore, the lithological character shows a gradual shift from mixed system (debrite, dolomite mudstone, mud with biogenic carbonate and mud-rich contourites) that dominated Stage 1 to mud-rich contourites which predominate during Stage 2 (Fig. 10). The Gulf of Cadiz and Le Danois CDS share similar morphologies since the Late Pliocene, where the previous sheeted drifts evolved towards plastered drifts and elongated, mounded and separated drifts with deep moats (Llave *et al*., 2007, 2011; Roque *et al*., 2012; Hernández-Molina *et al*., 2016b; Liu *et al*., 2019, 2020). Examples across the Mediterranean (particularly in the Adriatic and Alboran Sea), Porcupine Seabight, Argentine Margin and South China Sea indicate giant elongated mounded drifts were built during the Pliocene and Quaternary record (van Rooij *et al*., 2007; Hernández-Molina *et al*., 2010; Pellegrini *et al*., 2016; Miramontes *et al*., 2018, Kim *et al*., 2018; Yin *et al*., 2019; Juan *et al*., 2020). Across-high-latitude systems, giant contourite drifts with erosive moats are tied to significant bottom-current activity (Laberg *et al*., 2001; Kim *et al*., 2018). Therefore, the shift from sheeted to mounded drift clearly reflects a significant variation of the oceanic circulation patterns, which could have been triggered after the *EQD* (seismic horizon H3, 2.5-2.4 Ma). The period between H3 and H2 (2.4 to 0.7 Ma) are associated with considerable paleomoats, suggesting intensification of the MOW (Hernández-Molina *et al*., 2016b). This intensification is attributed to longer climatic cycles, since H3 and H2 coincide with important global cooling periods and sea-level falls (Bartoli *et al*., 2005; Miller *et al*., 2011; Fig. 12). The climatic changes along the Northern Hemisphere result from the intensifications of the Northern Hemisphere Glaciations (Bartoli *et al*., 2005), which would have led to changes in the thermohaline circulation and the dense MOW outflow would therefore form a more active circulation in the North Atlantic Ocean (Khélifi *et al*., 2009, 2014; Hernandez-Molina *et al*., 2014).

3. Maintenance stage (Middle Pleistocene to Present, 0.7 Ma)

The third and final stage of sedimentation led to the build-up of a plastered contourite drift from Middle Pleistocene to the present-day, which is represented by seismic unit U1 (Fig. 13). The change from the growing to the maintenance stage is marked by an important change in drift architecture (Fig. 3). The Sines Drift stacking pattern shifts from mounded to plastered, with higher sedimentation rates of 27 cm/ky (Expedition 339 Scientists, 2012). Site U1391 data shows that this change is marked by an increase of coarser-grained intervals and the presence of bigradational contourite successions. Stage 3 is also characterized by small precursory paleomoats along the upper continental slope (Fig. 6) and by MTDs across the western sector of the Sines Drift (Fig. 5). The MTDs along the west (Fig. 3) and at the foot of scarps (such as the PSS in Fig. 5), result from numerous slope failure events due to an almost constant supply of contouritic sediments across the margin. The constant sediment supply leads to oversteepening, overpressure and sediment shear stress near steep slopes (Neves et al., 2016; Teixeira et al., 2019). The same effect has been studied across the São Vicente Canyon and the adjacent plateaus, since the MOW effectively supplies and interacts with downslope processes across these features and has led to the formation of mixed or hybrid deposits (Serra et al., 2010; Mencaroni et al., 2020).

Similar to the Sines CDS, the Gulf of Cadiz CDS evolved towards mounded, separated drifts in the Quaternary (<2 Ma – present) with deep moats, contourite channels and proximal sandy deposits (Hernández-Molina et al., 2006; Llave et al., 2007). Le Danois CDS shares similar morphologies, characterized by mounded separated drifts with progradational reflections and deep U-shaped moats (Liu et al., 2019, 2020). However, the lack of contourite channels and proximal coarse-grained deposits in the Le Danois area indicates a more tabular water mass, probably due to its distal location. This outcome is also observed on the Sines CDS (Fig. 3), as well as on the West Portuguese CDS (Llave et al., 2019), and the Porcupine Seabight (Van Rooij et al., 2007). A similar and coeval change in drift construction has also been identified on the plastered drifts of the NW Mediterranean Sea (Miramontes et al., 2018) and South China Sea (Yin et al., 2019).

The development of the present-day MOW occurs during this last stage with three phases of MOW intensification, marked by two important discontinuities: the *MPD* (0.7-0.9 Ma, H6), the *LQD* (~0.4 Ma, H6A) and horizon H1$_A$ (~20 ka) (Fig. 12). Hernández-Molina et al. (2016b) attributes the MOW enhance of the MOW to the general climatic trend and the formation of the MOW pathways to tectonic constriction and deformation in the Gulf of Cadiz. The SW Portuguese margin shows the exact opposite during this last stage, with the absence of deformation and tectonic influence since the Middle Pleistocene

(Pereira and Alves, 2011; Hernández-Molina *et al*., 2016b; Fig. 3 and 9D). The maintenance stage is not affected by deformation, thus indicating that tectonics do not play a major role in the evolution of this depositional stage as in the Gulf of Cadiz. Across other continental margins in the Mediterranean Sea, as well as in the West and North Iberian Margins, increasing contourite deposition has been ascribed to enhanced paleo-current activity (Amelio and Martorelli, 2008; Van Rooij *et al*., 2010; Roque *et al*., 2012; Miramontes *et al*., 2018).

Since the Middle Pleistocene, three main phases of MOW intensification increased bottom-current strength has been determined. The first phase of MOW intensification is marked by the *MPD* (seismic horizon H1), which shows the change in drift morphology and the increase of sandier deposits (Fig. 10). The *MPD* is related to an important climatic change at 0.7-0.78 Ma (Hayward *et al*., 2009; Hernández-Molina *et al*., 2016b), marking a shift to longer glaciations and shorter interglaciations due to the growth of ice sheets in the Northern Hemisphere (Hayward *et al*., 2009; Lofi *et al*., 2016; Fig. 12). The second phase of MOW intensification is marked by the *LQD* (seismic horizon H1$_B$), which is also related to an important climatic change at ~0.4 Ma (Hayward *et al*., 2009; Lofi *et al*., 2016). The *LQD* coincides with a cold period in the Mediterranean region during the Pleistocene, formed by the advance of ice sheets towards lower latitudes (Hayward *et al*., 2009; Lofi *et al*., 2016). The third episode of MOW intensification is marked by horizon H1$_A$ (Fig. 12). This horizon coincides with the Last Glacial Period around 20 ka, indicating current enhancement before the transition towards the present circulation pattern of the MOW (Rogerson *et al*., 2005, 2006; García *et al*., 2009; Teixeira *et al*., 2020). The *MPD*, *LQD* and horizon H1$_A$ coincide with eustatic falls of the sea-level (Miller *et al*., 2005, 2011; Rogerson *et al*., 2012; Fig. 12). Teixeira et al. (2020) identified one sandy contourite bed at ~21.9 ka BP, which was tied to a significant intensification of the MOW.

Overall, the MOW was capable of constructing the Sines Drift on the left and its moat on the right side (Fig. 14). The Sines Drift did not migrate considerably since Late Miocene, as the flow pathway remained almost unchanged due to the paleo-relief constraints. Therefore, a long-term MOW current has consistently been flowing along the SW Portuguese Margin since that time until the present-day.

6.4. Plastered drifts: conceptual implications

Plastered drifts represent one of the most common depositional features associated with water mass circulation along continental slopes, forming a convex shape with predominant sediment accumulation in

29

the centre of the drift (Faugères *et al*., 1999; Faugères and Stow, 2008; Hernandez-Molina *et al* 2008b; Miramontes *et al*., 2019). They are defined as sheeted drifts 'plastered' against a gentle margin with a variable degree of mounding and alongslope elongation, despite being considered more mounded and at shallower depths than sheeted drifts, and also more subdued and smaller than giant, elongated mounded drifts (Faugères et al., 1999, Rebesco and Stow, 2001; Rebesco, 2005; Faugères and Stow, 2008; Rebesco *et al*., 2014). Plastered drifts are located along flatter or gently dipping seafloor along the upper, middle or lower continental slopes with averages of 10-100 km in length, 5-50 km in width and 300-1500 km in thickness over 50,000 km^2 (Faugères and Stow, 2008; Hernández-Molina *et al*., 2016a; Preu *et al*., 2013; Miramontes *et al*., 2018). Large elongated mounded drifts are more frequently found along the foot of the slope, or along the proximal continental rise of margins with steeper slopes and their average dimensions range between 100-1000 km in length, 10-100 km in width and 200-2000 km in thickness over 100,000 km^2 (Llave *et al*., 2007; Hernández-Molina *et al*., 2016b; Van Rooij *et al*., 2010; Roque *et al*., 2012; Liu *et al*., 2019, 2020). In contrast, sheeted drifts develop mostly on the abyssal plains with 100-2000 km in length, 100-2000 km in width and 300-3000 km in thickness over 1,000,000 km^2 (Faugères and Stow, 2008; Hernández-Molina *et al*., 2008a, 2016b). Pragmatically, there are some overlaps among all drift types, since all drifts are part of a continuous spectrum of deposits (Hernández-Molina *et al*., 2010, 2014). Some plastered drifts can actually be considered as sheeted drifts, whereas others must be considered as mounded, elongated drifts; regardless there is a continuity of examples in between these two end members (Rebesco *et al*., 2014).

The Sines Drift represents a plastered drift over the middle and lower continental slope with overall aggradational sheeted deposits and alongslope sedimentation (Fig. 3). It could be considered as the Type 3 from Miramontes *et al*. (2019) but its development and sedimentary stacking pattern allow us to decode the next important conceptual implications:

1) *Complex morphological evolution.* The Sines Drift evolved from a tabular to a mounded drift, before ending again as a more tabular shape. This evolution differs from adjacent continental margins (Llave *et al*., 2001, 2019; Van Rooij *et al*., 2010; Brackenridge *et al*. 2013; Hernandez-Molina *et al.*, 2016; Liu *et al*., 2019, 2020) where coeval drift evolved from sheeted to mounded morphologies.

2) *Contourite terrace.* The Sines Drift is characterized by a terrace along the middle slope, which is typical for this type of plastered drift across many margins (Viana, 2002; Hernández-Molina *et al*., 2009, 2010; 2016a; Preu *et al*., 2013; Llave *et al*., 2018; Miramontes *et al*., 2020). However, the

30

terrace is more commonly located at the top of the drift along the proximal part of the middle slope. Contourite terraces are usually associated with the influence of one water mass or with the pycnocline (interface) between water masses (Rebesco *et al*., 2014). Plastered drifts are usually formed below these terraces and they thicken outwards within zones of low bottom-current velocities, constrained upslope and downslope by higher current velocities (Miramontes *et al*., 2019). On the Sines Drift, the terrace is located in a distal and deeper part of the middle slope (1300-1900 m wd) and not in its proximal part (Figs. 1B and 6). The deeper location of the terrace is associated with the lower core (ML) of the MOW, which is enhanced at greater depths along the middle slope, in comparison with the upper core (MU) of the MOW (Fig. 1A), especially during glacial periods, precession minima and Greenland stadials (Llave *et al*., 2006; Sierro *et al*., 2020). Therefore, continental margins affected by one water mass with one core develop simple, wide terraces along the proximal part of the plastered drift, whereas margins where the water mass is composed by more than one main core, a more complex terrace and slope morphology should be expected.

3) *Sediment waves.* Sediment waves along the middle slope are parallel to lightly oblique to the general trend of the terrace. These sediment waves fields are commonly described along the upward termination of the contourite terrace (Hernández-Molina *et al*., 2010; Miramontes *et al*., 2019; Rovere *et al*., 2019), associated to oscillations of the pycnocline by internal or tidal waves (Rebesco *et al*., 2014; Miramontes *et al*., 2020). On the Sines Drift their distribution is wider across the middle slope, covering the terrace morphology and the northern sector.

4) *Occurrence of erosional features.* A variety of erosional features (channels, moats and furrows/valleys) is commonly described in association with more mounded, convex and/or tabular plastered drifts near steeper continental slopes or around high paleo-reliefs (Faugères *et al*., 1999, Rebesco and Stow, 2001; Rebesco, 2005; Rebesco *et al*., 2014), as identified across other continental slopes (Viana, 2002; Maldonado *et al*., 2005; Hernández-Molina *et al*., 2010, 2016a; Pellegrini *et al*., 2016; Llave *et al*., 2018; Miramontes *et al*., 2019, 2020; Mulder *et al*., 2019; Rovere *et al*., 2019; Liu *et al*., 2020). On the Sines Drift, several small-scale erosional features have been determined (Figs. 13 and 14), characterized by subtle morphologies and developed near the steep upper and lower continental slopes. This setting highlights the role of local bathymetric highs and of seafloor irregularities on locally enhancing bottom-currents and forming erosional features. In addition, secondary oceanographic processes across these locations would have amplified the average current

31

velocities (Rebesco *et al*., 2014; Chen *et al*., 2016, 2019; Zhang *et al*., 2016; Thran *et al*., 2018; Rovere *et al*., 2019; Yin *et al*., 2019).

The most significant outcome from the study of the Sines plastered drift is the fact that this kind of drift can evolve laterally and vertically towards different morphologies, denoting a complex sedimentary stacking pattern and changes in water mass behavior, even across short distances (dozens of kilometers) and relatively short periods of times (few Ma to Ky). Three types of plastered drifts could be considered (Fig. 15): A) a *sheeted plastered drift with a lateral erosive or non-depositional terrace*; B) a *mounded plastered drift associated with a large V- to U-shaped moat*, and C) a *tabular, concave plastered drift with a narrow V-shaped moat or valley*. The different types evolve towards each other and towards other drift types. Furthermore, the occurrence of downslope gravity-driven processes can lead to phased or synchronous interactions with alongslope bottom currents and form mixed turbidite-contourite systems, conditioning the occurrence of other deposits, such as reworked gravity deposits or interbedded MTDs. Therefore, the type and size of plastered drift (Fig. 15), as well as their spatial and temporal distribution, would be conditioned by the regional water masses circulation and its local hydrodynamic behavior and their interaction with seafloor irregularities, secondary oceanographic processes, and the tectonic and sedimentary background.

7. Conclusions

This work proposed an evolutionary model for the Sines CDS as well as the identification of its main driving and controlling mechanisms. All the results suggest that the Sines CDS had a complex evolution, controlled by several factors at different scales, from tectonics and bottom-current circulation to climatic-eustatic fluctuations, and by the interactions between them:

1. Three evolutionary phases were identified for the Sines Drift development: 1) *Onset and initial stage* (5.33 – 2.5 Ma) where a mixed system was built since the Late Miocene under an initially weak flowing MOW; 2) a *growing stage* (2.5 – 0.7 Ma), Early to Middle Quaternary in age, characterized by a mounded drift in the south and sheeted in the north with a succession of sinuous paleomoats along the east, built as a result of MOW enhancement; and 3) a *maintenance stage* from Mid-Pleistocene (0.7 Ma) till the present-day, characterized by the modern depositional (plastered drift with sandy-muddy contourite sequences) and erosional (moats) contourite features associated with three major events of MOW intensification;

2. The growth of the Sines Drift was mainly constrained by the Mesozoic paleo-reliefs in the Latest Miocene and by climatic-eustatic fluctuations in the Quaternary. The main controlling mechanisms have shifted in the long-term, however each mechanism operates at a different (time-) scale. This results in enhancements or recessions of the bottom-current (MOW), producing changes in drift morphology, stacking patterns and sedimentary facies;

3. The Sines Drift shares similar stratigraphic stacking patterns and morphological features with plastered drifts from other continental margins. But this drift evolves laterally and vertically towards different morphologies, denoting a complex sedimentary stacking pattern and changes in water mass behavior across short distances (dozens of km) and relatively short periods of times (few Ma to Ky). Future investigations using 3D seismic and well data are essential to better understand the complex variability of plastered drifts, its dominant sedimentary facies and the role of gravitational processes on their formation.

Acknowledgments

Figure Captions

Fig. 1. Bathymetric map of the Southwest Iberian Margin, presenting the main water masses (A) and morphological features (B). Water masses after Hernández-Molina *et al*., (2011, 2016). The global GEBCO (2019) data was used to fill in the gaps of the SWIM dataset. BS – Bow Spur; CDS – Contourite Depositional System; DS – Descobridores Seamounts; MPF – Marquês de Pombal Fault; MPP – Marquês

de Pombal Plateau; PAP – Príncipe de Avis Plateau; PAS – Príncipe de Avis Seamounts; PSF – Pereira de Sousa Fault; PSS – Pereira de Sousa Scarp; RLB – Rincão do Lebre Basin; SC – Setúbal Canyon; SD – Sines Drift; SH – Sines Hook; SVC – São Vicente Canyon.

Fig. 2. Geomorphologic map of the study area, showing the main physiographic domains and morphological features. BS – Bow Spur; CDS – Contourite Depositional System; DS – Descobridores Seamounts; MPP – Marquês de Pombal Plateau; PAP – Príncipe de Avis Plateau; PAS – Príncipe de Avis Seamounts; PSS – Pereira de Sousa Scarp; RLB – Rincão do Lebre Basin; SC – Setúbal Canyon; SD – Sines Drift; SH – Sines Hook; SVC – São Vicente Canyon.

Table 1. Acquisition parameters of each seismic survey: CONDRIBER, STEAM, BIGSETS and GSI (Alves *et al.,* 2000; Zitellini *et al.*, 2001; Informe Técnico Campaña MOWER, 2014).

Table 2. Main seismic units and discontinuities identified in this work and correlated with the main discontinuities and time intervals defined in previous studies.

Fig. 3. Un-interpreted (A) and interpreted (B) seismic line CL01E displaying the drift's asymmetric shape and MTDs identified in the west. U1 to U6 – seismic units; B and $H1_A$ to $H6_A$ – seismic horizons; HMTD – base of MTDs; S – seafloor horizon. F – faults; black arrows – reflections terminations; shaded areas – paleomoats; M – multiple. Line location in Figs. 1B and 2.

Fig. 4. Un-interpreted (A) and interpreted (B) section of seismic line CL04 showing paleomoats formed since seismic unit U3 and several MTDs in the upper units. U1 to U6 – seismic units; B and $H1_A$ to $H6_A$ – seismic horizons; S – seafloor horizon. F – faults; black arrows – reflections terminations; shaded areas – paleomoats; M – multiple. Line location in Figs. 1B and 2.

Fig. 5. Un-interpreted (A) and interpreted (B) seismic line BS19 shows MTDs accumulation related to the Pereira de Sousa escarpment and the correlation with Site U1391 stratigraphic discontinuities. U1 to U6 – seismic units; B and $H1_A$ to $H6_A$ – seismic horizons; HMTD – base of MTDs; S – seafloor horizon. F –

faults; black arrows – reflections terminations; shaded areas – paleomoats; M – multiple. Line location in Figs. 1B and 2.

Fig. 6. Un-interpreted (A) and interpreted (B) seismic line CL11, showing the paleomoats formed since seismic unit U3 and paleochannels affecting seismic units U4 to U6. U1 to U6 – seismic units; B and H1$_A$ to H6$_A$ – seismic horizons; HMTD – base of MTDs; S – seafloor horizon. F – faults; black arrows – reflections terminations; shaded areas – paleomoats; M – multiple. Line location in Figs. 1B and 2.

Fig. 7. Un-interpreted (A) and interpreted (B) section of seismic line UGI68 displaying well Pescada-1 and the B unconformity. B – seismic horizon; S – seafloor horizon. Line location in Figs. 1B and 2.

Fig. 8. Un-interpreted (A) and interpreted (B) section of seismic line BS19 with Site U1391 and the correlated discontinuities. H1$_B$, H1, H3 and H4 – seismic horizons; S – seafloor horizon.

Fig. 9. Isopach map of the Sines Drift total thickness (comprising seismic units U1 to U6) and isobath maps for the main horizons B, H3 and H1; **h1** and **h2** correspond to horsts and **g1** to a graben; D1 to D3 mark the main depocenters; PAP – Príncipe de Avis Plateau; PAS – Príncipe de Avis Seamounts; PSF – Pereira de Sousa Fault; RLB – Rincão de Lebre Basin; SD – Sines Drift. Equidistance: 250 ms**.**

Fig. 10. U1391 logging and physical properties, from left to right: resistivity (ohm.m); HROM density (g/cm^3); gamma ray (GAPI); velocity (km/s) with DSI Tool; natural gamma ray total counts (cps); magnetic susceptibility (instrumental units); color reflectance (a*, b* and L*); U1391A and U1391B major lithology (average and maximum) grain size rank; lithostratigraphic column with the seismic units identified on this study and location of the high-resolution photos (A, B and C) shown in Fig. 11. Blue lines – seismic horizons; gray lines – coarse-grained beds.

Fig. 11. High-resolution photos taken onboard the IODP Expedition 339 Site U1391 showing selected examples of the main sedimentary facies for contourites (A), debrite (B) and dolomite mudstone (C).

35

Fig. 12. Late Miocene to Quaternary evolution of the Sines Drift, characterized by three growth stages with distinct seismic and lithological character. Paleogeographic events, glacio-eustatic sea-level changes and transgressive-regressive cycles associated with the formation of the Sines Drift are also included. Glacio-eustatic data extracted from Haq *et al*. (1987), Llave *et al*. (2007), Hernández-Molina *et al*. (2016), Ogg and Ogg (2008), De Boer *et al*. (2010) and Miller *et al*. (2011), and sedimentation rates after Expedition 339 Scientists (2012). *EQD – Early Quaternary Discontinuity*; *MPD – Middle Pleistocene Discontinuity*; *LPD – Late Pliocene Discontinuity; LQD – Late Quaternary*.

Fig. 13. Representation of the depositional evolution of the Sines Drift, with possible changes in MOW intensification, drift architecture and the main factors that control contourite formation: tectonics, paleomorphology, paleoceanography and slope instability. PSF – Pereira de Sousa Fault; PSS – Pereira de Sousa Scarp.

Fig. 14. Model of the Southwest Portuguese Margin and its main physiographic domains and morphologic features. PSS – Pereira de Sousa Scarp.

Fig. 15. Conceptual model for the three main types of plastered drifts: A) Type 1 represents a sheet to wedge plastered drift topped by a terrace in its proximal sector; B) Type 2 characterizes a mounded plastered drift with an adjacent V-shaped moat; and C) Type 3 represents a tabular, concave plastered drift with an adjacent V-shaped moat.

References

Alves, T.M., Gawthorpe, R.L., Hunt, D., Monteiro, J.H., 2000. Tertiary evolution of the São Vicente and Setúbal submarine canyons, Southwest Portugal: insights from seismic stratigraphy. Ciências da Terra, 14, 243-256.

Alves, T.M., Gawthorpe, R.L., Hunt, D.W., Monteiro, J.H., 2002. Jurassic tectono-sedimentary evolution of the Northern Lusitanian Basin (offshore Portugal). Mar. Petrol. Geol. 19, 727-754.

Alves, T.M., Gawthorpe, R.L., Hunt, D.W., Monteiro, J.H., 2003. Cenozoic tectono-sedimentary evolution of the western Iberian margin. Mar. Geol. 195, 75-108.

Alves, T.M., Moita, C., Sandes, F., Cunha, C., Monteiro, J.H., Pinheiro, L.M., 2006. Mesozoic-Cenozoic evolution of North Atlantic continental-slope basins: The Peniche basin, western Iberian margin. AAPG Bulletin 90 (1), 31-60.

Alves, T.M., Moita, C., Cunha, T., Ullnaess, M., Myklebust, R., Monteiro, M.J., Manuppella, G., 2009. Diachronous evolution of late Jurassic-cretaceous continental rifting in the northeast Atlantic (west Iberian margin). Tectonics 28, 32.

Alves, T.M., Cunha, T.A., Moita, C., Terrinha, P., Hipólito, M.J., Manupella, G., 2013. A evolução de bacias sedimentares tipo-rift em margens continentais passivas: o exemplo da Margem Ocidental Ibérica. In: Dias, R., Araújo, A., Terrinha, P., Kullberg, J.C. (Eds.), Geologia de Portugal, Volume II: Geologia Meso-cenozóica de Portugal, Escolar Editora, Lisboa, III.4., 349-404.

Ambar, I., Howe, M.R., 1979. Observations of the Mediterranean outflow-II. The deep circulation in the vicinity of the Gulf of Cadiz. Deep-Sea Res. 26(A), 555-568.

Ambar, I., Serra, N., Brogueira, M.J., Cabeçadas, G., Abrantes, F., Freitas, P., Gonçalves, C., Gonzalez, N., 2002. Physical, chemical and sedimentological aspects of the Mediterranean outflow off Iberia. Deep-Sea Res. Part I: Oceanogr. Res. Pap. 49, 4163-4177.

Ambar, I., Serra, N., Neves, F., Ferreira, T., 2008. Observations of the Mediterranean undercurrent and eddies in the gulf of cádiz during 2001. J. Mar. Syst. 71 (1-2), 195-220.

Amelio, M., Martorelli, E., 2008. Seismo-stratigraphic characters of paleocontourites along the Calabro-Tyrrhenian margin (Southern Tyrrhenian Sea). Mar. Geol. 252 (3-4), 141-149.

Azerêdo, A.C., Duarte, L.V., Henriques, M.H. and Manupella, G., 2003. Da dinâmica continental no Triásico aos mares do Jurássico Inferior e Médio. Cadernos de Geologia de Portugal, Instituto Geológico e Mineiro, Lisboa, 43.

Bache, F., Popescu, S.-M., Rabineau, M., Gorini, C., Suc, J.-P., Clauzon, G., Olivet, J.-L., Rubino, J.-L., Melinte-Dobrinescu, M., Estrada, F., Londeix, L., Armijo, R., Meyer, B., Jolivet, L., Jouannic, G., Leroux, E., Aslanian, D., Tadeu Dos Reis, A., Mocochain, L., Dumurdzanov, N., Zagorchev, I., Lesic, V., Tomic, D., Catagay, M., Brun, J.-P., Sokoutis, D., Csato, I., Ucarkus, G., Cakir, Z., 2012. A two step process for the reflooding of the Mediterranean after the Messinian Salinity Crisis. Basin Res. 24, 125-153.

Baringer, M., Price, J., 1997. Mixing and spreading of the Mediterranean outflow. J. Phys. Oceanogr. 27 (8), 1654-1677.

Bartoli, G., Sarnthein, M., Weinelt, M., Erlenkeuser, H., Garbe-Schönberg, D., Lea, D.W., 2005. Final closure of panama and the onset of northern hemisphere glaciation. Earth Planet. Sci. Lett. 237, 33-44.

Batista., L., 2009. Cartografia da Deformação Tectónica de Idade Pliocénica e Quaternária na Planície Abissal do Tejo, Talude e Plataforma Continental Adjacentes com Base na Interpretação de Perfis Sísmicos de Reflexão e Batimetria Multifeixe. MSc thesis, Universidade de Lisboa, Lisboa, 84.

Bender, V.B., Hanebuth, T.J.J., Mena, A., Baumann, K.H., Francés, G., Von Dobeneck, T., 2012. Control of sediment supply, palaeoceanography and morphology on late Quaternary sediment dynamics at the Galician continental slope. Geo-Mar. Lett. 32, 313-335.

Béthoux, J.-P., Pierre, C., 1999. Mediterranean functioning and sapropel formation: respective influences of climate and hydrological changes in the Atlantic and the Mediterranean. Mar. Geol. 153, 29-39.

Bower, A., Serra, N., Ambar, I., 2002. Structure of the Mediterranean undercurrent and Mediterranean water spreading around the southwestern Iberian Peninsula. J. Geophys. Res. 107 (C10), 1-19.

Brackenridge, R.A., Hernández-Molina, F.J., Stow, D.A.V., Llave, E., 2013. A Pliocene mixed contourite-turbidite system offshore the Algarve Margin, Gulf of Cadiz: Seismic response, margin evolution and reservoir implications. Mar. Petrol. Geol. 46, 36-50.

Cacho, I., Grimalt, J.O., Sierro, F.J., Shackleton, N.J., Canals, M., 2000. Evidence of enhanced Mediterranean thermohaline circulation during rapid climatic coolings. Earth Planet. Sci. Lett. 183, 417-429.

Cacho, I., Grimalt, J.O., Canals, M., 2002. Response of the Western Mediterranean Sea to rapid climatic variability during the last 50,000 years: a molecular biomarker approach. J. Mar. Syst. 33-34, 253-272.

Cacho, I., Shackleton, N., Elderfield, H., Sierro, F.J., Grimaltd, J.O., 2006. Glacial rapid variability in deep-water temperature and δ18O from the Western Mediterranean Sea. Quat. Sci. Rev. 25, 3294-3311.

Capella, W., Barhoun, N., Flecker, R., Hilgen, F.J., Kouwenhoven, T., Matenco, L.C., Sierro, F.J., Tulbure, M.A., Yousfi, M.Z., Krijgsman, W., 2018. Palaeogeographic evolution of the late Miocene Rifian Corridor (Morocco): Reconstructions from surface and subsurface data. Earth Sci. Rev. 180, 37-59.

Capella, W., Flecker, R., Hernández-Molina. F.J., Simon, D., Meijer, P.T., Rogerson, M., Sierro, F.J., Krijgsman, W., 2019. Mediterranean isolation predonditioning the Earth System for late Miocene climate cooling. Sci. Rep. 9, 3795.

Chen, H., Xie, X., Zhang, W., Shu, Y., Wang, D., Vandorpe, T., Van Rooij, D., 2016. Deep-water sedimentary systems and their relationship with bottom currents at the intersection of Xisha Trough and Northwest Sub-Basin, South China Sea. Mar. Geol. 378, 101-113.

Chen, H., Zhang, W., Xie, X., Ren, J., 2019. Sediment dynamics driven by contour currents and mesoscale eddies along continental slope: A case study of the northern South China Sea. Mar. Geol. 409, 48-66.

Cita, M. B., 2001. The Messinian salinity crisis in the Mediterranean. In: Briegel U., Xiao, W. (Eds.), Paradoxes in Geology. Elsev. Sci. 353-360.

Criado-Aldeanueva, F., García-Lafuente, J., Vargas, J., Del Río, J., Vázquez, A., Reul, A., Sánchez, A., 2006. Distribution and circulation of water masses in the Gulf of Cadiz from in situ observations. Deep-Sea Res. Part II, 53 (11-13), 1144-1160.

Duarte, J.C., Rosas, F.M., Terrinha, P., Schellart, W.P., Bourelier, D., Gutscher, M.-A., Ribeiro, A., 2013. Are subduction zones invading the Atlantic? Evidence from the southwest Iberia margin. Geology 41, 839-842.

Duggen, S., Hoernle, K., Van den Bogaard, P., Rüpke, L., Morgan, J.P., 2003. Deep roots of the Messinian salinity crisis. Nature 422 (6932), 602-606.

Ercilla, G. Casas, D. Vázquez, J.T., Iglesias, J., Somoza, L., Juan, C., Medialdea, T., León, R., Estrada, F., García-Gil, S., Farran, M., Bohoyo, F., García, M., Maestro, A., ERGAP Project and Cruise Teams, 2011. Imaging the recent sediment dynamics of the Galicia Bank region (Atlantic, NW Iberian Peninsula). Mar. Geophys. Res. 32 (1-2), 99-126.

Expedition 339 Scientists, 2012. Mediterranean outflow: environmental significance of the Mediterranean outflow water and its global implications. Proceedings of the Integrated Ocean Drilling Program, Scientific Results 339, 106.

Faugères, J.-C., Stow, D.A.V., 2008. Contourite drifts: nature, evolution and controls. In: Rebesco, M., Camerlenghi, A. (Eds.), Contourites. Dev. Sedimentol., Elsevier, Amsterdam, 60, 259-288.

Faugères, J.C., Frappa, M. Gonthier, E., Grousset, E., 1985a. Impact de la veine d'eau mediterraneenne sur la sedimentation de la marge sud et ouest iberique au Quaternaire recent. Bulletin - Institut de Geologie du Bassin d'Aquitaine 37, 259-287.

Faugères, J.C., Crémer, M., Monteiro, H., Gaspar, L., 1985b. Essai de reconstitution des processus d'édification de la ride sédimentaire de Faro (marge sud-portugaise). Bulletin - Institut de Geologie du Bassin d'Aquitaine 37, 229-258.

Faugères, J.-C., Stow, D.A.V., Imbert, P., Viana, A. R., 1999. Seismic features diagnostic of contourite drifts. Mar. Geol. 162, 1-38.

Figueiredo, P. M., Cabral, J., Rockwell, T. K., 2013. Recognition of Pleistocene marine terraces in the southwest of Portugal (Iberian Peninsula) evidences of regional Quaternary uplift. Annals Geopys. 56, 19.

Flecker, R., Krijgsman, W., Capella, W., Martins, C., De, C., Demitrieva, E., Mayser, J.P., Marzocchi, A., Modestu, S., Ochoa Lozano, D., Simon, D., Tulbure, M., Van den Berg, B., Van der Schee, M., de Lange, G., Ellam, R., Govers, R., Gutjahr, M., Hilgen, F., Kouwenhoven, T., Lofi, J., Meijer, P., Sierro, F.J., Bachiri, N., Barboun, N., Chakor Alami, A., Chacon, B., Flores, J.A., Gregory, J., Howard, J., Lunt, D., Ochoa, M., Pancost, R., Vincent, S., Yousfi, M. Z., 2015.

Evolution of the late Miocene Mediterranean-Atlantic gateways and their impact on regional and global environmental Change. Earth Sci. Rev. 150, 365-392.

Flinch, J., Vail, P., 1998. Plio-Pleistocene sequence stratigraphy and tectonics of the Gibraltar Arc. In: De Graciansky, P., Hardenbol, J., Jacquin, T., Vail, P. (Eds.), Mesozoic and Cenozoic Sequence Stratigraphy of European Basins, Society for Sedimentary Geology 60, 199-208.

García, M., Hernández-Molina, F.J., Llave, E., Stow, D.A.V., León, R., Fernández-Puga, M.C., Díaz del Río, V., Somoza, L., 2009. Contourite erosive features caused by the Mediterranean outflow water in the gulf of Cadiz: Quaternary tectonic and oceanographic implications. Mar. Geol. 257, 24-40.

Garcia-Castellanos, D., Estrada, F., Jiménez-Munt, I., Gorini, C., Fernàndez, M., Vergés, J., De Vicente, R., 2009. Catastrophic flood of the Mediterranean after the Messinian salinity crisis. Nature 462 (7274), 778-781.

General Bathymetric Chart of the Oceans, 2019. GEBCO 2019 Grid. www.gebco.net.

Gutscher, M.-A., Malod, J., Rehault, J.-P., Contrucci, I., Klingelhoefer, F., Mendes-Victor, L., Spakman, W., 2002. Evidence for active subduction beneath Gilbraltar. Geology 30 (2), 1071-1074.

Gutscher, M.-A., Dominguez, S., Westbrook, G.K., Le Roy, P., Rosas, F., Duarte, J.C., Terrinha, P., Miranda, J.M., Graindorge, D., Gailler, A., Sallares, V., Bartolome, R., 2012. The Gilbraltar subduction: A decade of new geophysical data. Tectonophysics 574-575, 72-91.

Haq, B.U., Hardenbol, J., Vail, P.R., 1987. Chronology of Fluctuating Sea Levels Since the Triassic. Science 235, 1156-1167.

Hayward, B.W., Sabaa, A.T., Kawagata, S., Grenfell, H.R., 2009. The Early Pliocene recolonisation of the deep Mediterranean Sea by benthic foraminifera and their pulsed Late Pliocene-Middle Pleistocene decline. Mar. Micropaleo. 71, 97-112.

Hernández-Molina, F.J., Llave, E., Somoza, L., Fernández-Puga, M.C., Maestro, A., León, R., Barnolas, A., Medialdea, T., García, M., Vázquez, J.T., Díaz del Río, V., Fernández- Salas, L.M., Lobo, F., Alveirinho Dias, J.M., Rodero, J., Gardner, J., 2003. Looking for clues to paleoceanographic imprints: a diagnosis of the gulf of Cadiz contourite depositional systems. Geology 31 (1), 19-22.

Hernández-Molina, F.J., Llave, E., Stow, D.A.V., García, M., Somoza, L., Vázquez, J.T., Lobo, F.J., Maestro, A., Díaz del Río, V., León, R., Medialdea, T., Gardner, J., 2006. The contourite depositional system of the gulf of Cadiz: a sedimentary model related to the bottom current activity of the Mediterranean outflow water and its interaction with the continental margin. Deep-Sea Res. Part II. Top. Stud. Oceanogr. 53 (11-13), 1420-1463.

Hernández-Molina, F.J., Maldonado, A., Stow, D.A.V., 2008a. Abyssal Plain Contourites. In: Rebesco, M. Camerlenghi, A. (Eds.), Contourites. Dev. Sedimentol., Elsevier, Amsterdam, 60, 347-378.

Hernández-Molina, F.J., Stow, D.A.V., Llave, 2008b. Continental slope contourites, In: Rebesco, M., Camerlenghi, A. (Eds.), Contourites. Dev. Sedimentol., Elsevier, Amsterdam, 60, 379-408.

Hernández-Molina, F.J., Paterlini, M., Somoza, L., Violante, R., Arecco, M.A., de Isasi, M., Rebesco, M., Uenzelmann-Neben, G., Neben, S., Marschall, P., 2010. Giant mounded drifts in the Argentine Continental Margin: Origins, and global implications for the history of thermohaline circulation. Mar. Petrol. Geol. 27, 1508-1530.

Hernández-Molina, F.J., Serra, N., Stow, D.A.V., Llave, L., Ercilla, E., Van Rooij, D., 2011. Along-slope oceanographic processes and sedimentary products around the Iberian margin. Geo-Mar. Lett. 31 (5), 315-341.

Hernández-Molina, F.J., Stow, D.A.V., Alvarez-Zarikian, C., Acton, G., Bahr, A., Balestra, B., Ducassou, E., Flood, R., Flores, J.A., Furota, S., Grunert, P., Hodell, D., Jimenez-Espejo, F., Kim, J.K., Krissek, L., Kuroda, J., Li, B., Llave, E., Lofi, J., Lourens, L., Miller, M., Nanayama, F., Nishida, N., Richter, C., Roque, C., Pereira, H., Sanchez Goñi, M.F., Sierro, F.J., Singh, A.D., Sloss, C., Takashimizu, Y., Tzanova, A., Voelker, A., Williams, T., Xuan, C., 2014. Onset of Mediterranean outflow into the north Atlantic. Science 344, 1244-1250.

Hernández-Molina, F.J., Soto, M., Piola, A.R., Tomasini, J., Preu, B., Thompson, P., Badalini, G., Creaser, A., Violante, R.A., Morales, E., Paterlini, M., De Santa Ana, H., 2016a. A contourite depositional system along the Uruguayan continental margin: Sedimentary, oceanographic and paleoceanographic implications. Mar. Geol. 378, 333-349.

Hernández-Molina, F.J., Sierro, F.J., Llave, E., Roque, C., Stow, D.A.V., Williams, T., Lofi, J., Van der Schee, M., Arnáiz, A., Ledesma, S., Rosales, C., Rodríguez-Tovar, F.J., Pardo-Igúzquiza, E., Brackenridge, R.E., 2016b. Evolution of the gulf of Cadiz margin and southwest Portugal contourite depositional system: Tectonic, sedimentary and paleoceanographic implications from IODP expedition 339. Mar. Geol. 377, 7-39.

Hsü, K., Ryan, W., Cita, M., 1973. Late Miocene dessication of Mediterranean. Nature 242 (5395), 240-244.

Hunter, S.E., Wilkinson, D., Louarn, E., McCave, I.N., Rohling, E., Stow, D.A.V., Bacon, S., 2007a. Deep Western Boundary Current dynamics and associated sedimentation on the Eirik Drift, Southern Greenland Margin. Deep-Sea Res. Part I: Oceanogr. Res. Pap. 54, 2036-2066.

Hunter, S.E., Wilkinson, D., Stanford, J., Stow, D.A.V., Bacon, S., Akhmetzhanov, A.M., Kenyon, N.H., 2007b. The Eirik Drift: a longterm barometer of north Atlantic deepwater flux south of Cape Farewell, Greenland. In: Viana, A., Rebesco, M. (Eds.), Economic and Paleoceanographic Importance of Contourites. Geol. Soc. London Spec. Publ. 276, 245-264.

Juan, C., Ercilla, G., Hernández-Molina, F.J., Estrada, F., Alonso, B., Casas, D., García, M., Farran, M., Llave, E., Palomino, D., Vázquez, T.J., Medialdea, T., Gorini, C., D'Acremont, E., Moumni, B. E., Ammar, A., 2016. Seismic evidence of current-controlled sedimentation in the Alboran Sea during the Pliocene and Quaternary: Palaeoceanographic implications. Mar. Geol. 378, 292-311.

Juan, C., Ercilla, G., Estrada, F., Alonso, B., Casas, D., Vázquez, J.T., D'Acremont, E., Medialdea, T., Hernández-Molina, F.J., Gorini, C., Moumni, B., Valencia, J., 2020. Multiple factors controlling the deep marine sedimentation of the Alboran Sea (SW Mediterranean) after the Zanclean Atlantic Mega-flood. Mar. Geol. 423, 106138.

Kim, S., De Santis, L., Hong, J.K., Cottlere, D., Petronio, L., Colizza, E., Kim, Y.-G., Kang, S.-G., Kim, H. J., Kim, S., Wardell, N., Geletti, R., Bergamasco, A., McKay, R., Jin, Y.K., Kang, S.-H., 2018. Seismic stratigraphy of the Central Basin in northwestern Ross Sea slope and rise, Antarctica: Clues to the Late Cenozoic ice-sheet dynamics and bottom-current activity. Mar. Geol. 395, 363-379.

Khélifi, N., Sarnthein, M., Andersen, N., Blanz, T., Frank, M., Garbe-Schönberg, D., Haley, B.A., Stumpf, R., Weinelt, M., 2009. A major and long-term Pliocene intensification of the Mediterranean outflow, 3.5-3.3 Ma ago. Geology 37, 811-814.

Khélifi, N., Sarnthein, M., Frank, M., Andersen, N., Garbe-Schönberg, D., 2014. Late Pliocene Variations of the Mediterranean Outflow. Mar. Geol. 357, 182-194.

Laberg, J.S., Dahlgren, T., Vorren, T., Haflidason, H., Bryn, P., 2001. Seismic analyses of Cenozoic contourite drift development in the Northern Norwegian Sea. Mar. Geophys. Res. 22, 401-416.

Louarn, E., Morin, P., 2011. Antarctic Intermediate Water influence on Mediterranean Sea Water outflow. Deep-Sea Res. Part I, 58 (9), 932-942.

Liu, S., Van Rooij, D., Vandorpe, T., González-Pola, C., Ercilla, G., Hernández-Molina, F.J., 2019. Morphological features and associated bottom-current dynamics in the Le Danois Bank region (southern Bay of Biscay, NE Atlantic): A model in a topographically constrained small basin. Deep-Sea Res. Part I: Oceanogr. Res. Pap. 149, 1-17.

Liu, S., Hernández-Molina, F.J., Ercilla, G., Van Rooij, D., 2020. Sedimentary evolution of the Le Danois contourite drift systems (southern Bay of Biscay, NE Atlantic): A reconstruction of the Atlantic Mediterranean Water circulation since the Pliocene. Mar. Geol. (in press).

Llave, E., Hernández-Molina, F.J., Somoza, L., Díaz del Río, V., Stow, D.A.V., Maestro, A., Alveirinho Dias, J.M., 2001. Seismic stacking pattern of the faro-albufeira contourite system (gulf of

Cadiz): a Quaternary record of paleoceanographic and tectonic influences. Mar. Geophys. Res. 22, 487-508.

Llave, E., Schönfeld, J., Hernández-Molina, F.J., Mulder, T., Somoza, L., Díaz del Río, V.I., Sánchez-Almazo, I., 2006. High-resolution stratigraphy of the Mediterranean outflow contourite system in the gulf of Cadiz during the late Pleistocene: the impact of Heinrich events. Mar. Geol. 227, 241-262.

Llave, E., Hernández-Molina, F.J., Stow, D., Fernández-Puga, M.C., García, M., Vázquez, J.T., Maestro, A., Somoza, L., Díaz del Río, V., 2007. Reconstructions of the Mediterranean outflow water during the Quaternary since the study of changes in buried mounded drift stacking pattern in the gulf of Cadiz. Mar. Geophys. Res. 28 (4), 379-394.

Llave, E., Matias, H., Hernández-Molina, F.J., Ercilla, G., Stow, D.A.V., Medialdea, T., 2011. Pliocene–Quaternary contourites along the northern gulf of Cadiz margin: sedimentary stacking pattern and regional distribution. Geo-Mar. Lett. 31 (5-6), 377-390.

Llave, E., Hernández-Molina, F.J., Ercilla, G., Roque, C., Van Rooij, D., García, M., Juan, C., Mena, A., Brackenridge, R., Jané, G., Stow, D., Gómez-Ballesteros, M., 2015. Bottom current processes along the Iberian continental margin. Boletín Geológico y Minero 126 (2-3), 219-256.

Llave, E., Jané, G., Maestro, A., López-Martínez, J., Hernández-Molina, F.J., Mink, S., 2018. Geomorphological and sedimentary processes of the glacially influenced northwestern Iberian continental margin and abyssal plains. Geomorphology 312, 60-85.

Llave, E., Hernández-Molina, F.J, García, M., Ercilla, G., Roque, C., Juan, C., Mena, A., Preu, B., Van Rooij, D., Rebesco, M., Brackenridge, R., Jané, G., Gómez-Ballesteros, M., Stow, D., 2019. Contourites along the Iberian continental margin: conceptual and economic implications. In: McClay, K.R., Hammerstein, J.A. (Eds.) Passive Margins: Tectonics, Sedimentation and Magmatism. Geol. Soc. London Spec. Publ. 476, 1-34.

Lofi, J., Voelker, A. H.L., Ducassou, E., Hernández-Molina, F.J., Sierro, F.J., Bahr, A., Galvani, A., Lourens, L.J., Pardo-Igúzquiza, E., Pezard, P., Rodríguez-Tovar, F.J., Williams, T., 2016. Quaternary chronostratigraphic framework and sedimentary processes for the Gulf of Cadiz and Portuguese Contourite Depositional Systems derived from Natural Gamma Ray records. Mar. Geol. 377, 40-57.

Maldonado, A., Somoza, L., Pallares, L., 1999. The betic orogen and the Iberian-African boundary in the gulf of Cadiz, geological evolution central north Atlantic. Mar. Geol. 155, 9-43.

Maldonado, A., Barnolas, A., Bohoyo, F., Escutia, C., Galindo-Zaldívar, J., Hernández-Molina, F.J., Jabaloy, A., Lobo, F.J., Hans Nelson, C., Rodríguez-Fernández, J., Somoza, L., Vázquez, J.-T., 2005. Miocene to Recent contourite drifts development in the northern Weddell Sea (Antarctica). Glob. Planet. Chang. 45, 99-129.

Matias, H., 2002. Interpretação tectono-estratigráfica da área do Marquês de Pombal, a oeste do cabo de São Vicente. MSc thesis, Universidade de Lisboa, Lisboa, 114.

Mencaroni, D., Urgeles, R., Camerlenghi, A., Llopart, J., Ford, J., Serra, C.S., Meservy, W., Gràcia, E., Rebesco, M., Zitellini, N., 2020. Interaction between contour currents and submarine canyons: depositional products and significance for mass-wasting processes, Gulf of Cadiz, NE Atlantic. Sedimentology. Manuscript submitted for publication.

Miller, K.G., Kominz, M.A., Browning, J.V., Wright, J.D., Mountain, G.S., Katz, M.E., Sugarman, P.J., Cramer, B.S., Christie-Blick, N., Pekar, S.F., 2005. The phanerozoic record of global sea-level change. Science 310, 1293-1298.

Miller, K.G., Mountain, G.S., Wright, J.D., Browning, J.V., 2011. A 180-million-year record of sea level and ice volume variations from continental margin and deep-sea isotopic records. Oceanography 24 (2), 40-53.

Miramontes, E., Cattaneo, A., Jouet, G., Théreau, E., Thomas, Y., Rovere, M., Cauquil, E., Trincardi, F. , 2016. The Pianosa Contourite Depositional System (Northern Tyrrhenian Sea): Drift morphology and Plio-Quaternary stratigraphic evolution. Mar. Geol. 378, 20-42.

Miramontes, E., Garziglia, S., Sultan, N., Jouet, G., Cattaneo, A., 2018. Morphological control of slope instability in contourites: a geotechnical approach. Landslides 15, 1085-1095.

Miramontes, E., Garreau, P., Caillaud, M., Jouet, G., Pellen, R., Hernández-Molina, F.J., Clare, M.A., Cattaneo, A., 2019. Contourite distribution and bottom currents in the NW Mediterranean Sea: Coupling seafloor geomorphology and hydrodynamic modelling. Geomorphology 333, 43-60.

Miramontes, E., Jouet, G., Thereau, E., Bruno, M., Penven, P., Guerin, C., Le Roy, P., Droz, L., Jorry, S., Hernández-Molina, F.J., Thiéblemont, A., Jacinto, R.S., Cattaneo, A., 2020. The impact of interval waves on upper continental slopes: insigths from the Mozambican margin (southwest Indian Ocean). Earth Surf. Process. Landforms 45, 1469-1482.

Mougenot, D., 1976. Géologie du plateau continental portugaise (entre le cap Carvoeiro et le cap de Sines). Fascicule 1 et 2, Thèse 3ème cycle. Univ. Rennes, 76. (not published)

Mougenot, D., Monteiro, J.H., Dupeuble, P.A., Malod, J.A., 1979. La marge continentale sud-portugaise: évolution structurale et sédimentaire. Ciências da Terra 5, 223-246.

Mulder, T., Voisset, M., Lecroart, P., Le Drezen, E., Gonthier, E., Hanquiez, V., Faugères, J.-C., Habgood, E., Hernández-Molina, F.J., Estrada, F., Llave, E., Poirier, D., Gorini, C., Fuchey, Y., Voelker, A., Freitas, P., Lobo Sánchez, F., Fernández, L.M., Morel, J., 2003. The gulf of Cadiz: an unstable giant contouritic levee. Geo-Mar. Lett. 23 (1), 7-18.

Mulder, T., Gonthier, E., Lecroart, P., Hanquiez, V., Marchès, E., Voisset, M., 2009. Sediment failures and flows in the Gulf of Cadiz (eastern Atlantic). Mar. Petrol. Geol. 26 (5), 660-672.

Mulder, T., Ducassou, E., Hanquiez, V., Principaud, M., Fauquembergue, K., Tournadour, E., Chabaud, L., Reijmer, J., Recouvreur, A., Gillet, H., Borgomano, J., Schmitt, A., Moal, P., 2019. Contour current imprints and contourite drifts in the Bahamian archipelago. Sedimentology 66, 1192-1221.

Nelson, C.H., Baraza, J., Maldonado, A., 1993. Mediterranean undercurrent sandy contourites Gulf of Cadiz, Spain. Sed. Geol. 82, 103-131

Nelson, C.H., Baraza, J., Rodero, J., Maldonado, A., Escutia, C., Barber Jr., J.H., 1999. Influence of the Atlantic inflow and Mediterranean outflow currents on late Pleistocene and Holocene sedimentary facies of gulf of Cadiz continental margin. Mar. Geol. 155, 99-129.

Neves, M.C., Terrinha, P., Afilhado, A., Moulin, M., Matias, L., Rosas, F., 2009. Response of a multi-domain continental margin to compression: study from seismic reflection-refraction and numerical modelling in the Tagus Abyssal Plain. Tectonophysics 468, 113-130.

Neves, M.C., Roque, C., Luttrell, K.M., Vázquez, J.T., Alonso, B., 2016. Impact of sea-level rise on earthquake and landslide triggering offshore the Alentejo margin (SW Iberia). Geo-Mar. Lett. 36, 415-424.

Ogg, J., Ogg, G., 2008. Neogene-Late Oligocene (0-33 Ma time-slice). Subcommission for Stratigraphic Information. Accessed at: http://stratigraphy.science.purdue.edu/charts/educational.html on 15/09/2016.

Pellegrini, C., Maselli, V., Trincardi, F., 2016. Pliocene–Quaternary contourite depositional system along the south-western Adriatic margin: changes in sedimentary stacking pattern and associated bottom currents. Geo-Mar. Lett. 36, 67–79

Pereira, R., Alves, T.M., 2010. Multiphased syn-rift segmentation on the SW Iberian margin. II Central and North Atlantic Conjugate Margins Conference, Lisbon, Portugal, 224-227.

Pereira, R., Alves, T.M., 2011. Margin segmentation prior to continental break-up: a seismic–stratigraphic record of multiphased rifting in the North Atlantic. Tectonophysics 505, 17-34.

Pereira, R., Alves, T. M., 2013. Crustal deformation and submarine canyon incision in a Meso-Cenozoic first-order transfer zone (SW Iberia, North Atlantic Ocean). Tectonophysics 601, 148-162.

Pinheiro, L.M., Wilson, R.C.L., Pena dos Reis, R., Whitmarsh, R.B., Ribeiro, A., 1996. The Western Iberia Margin: A Geophysical and Geological overview. In: Whitmarsh, R.B., Sawyer, D.S., Klaus, A., Masson, D.G. (Eds.), Proceedings of the Ocean Drilling Program, Scientific Results, 149, 3-23.

Preu, B., Hernández-Molina, F.J., Violante, R., Piola, A.R., Paterlini, C.M., Schwenk, T., Voigt, I., Krastel, S., Spiess, V., 2013. Morphosedimentary and hydrographic features of the northern Argentine margin: The interplay between erosive, depositional and gravitational processes and its conceptual implications. Deep-Sea Res. I 75, 157-174.

Rasmussen, E.S., Lomholt, S., Andersen, C., Vejbæk, O.V., 1998. Aspects of the structural evolution of the Lusitanian Basin in Portugal and the shelf and slope area offshore Portugal. Tectonophysics 300, 199-225.

Rebesco, M., 2005. Contourites. In: Richard, C., Selley, R.C., Cocks. L.R., Plimer, I.R. (Eds.), Encyclopedia of Geology, Elsevier, London, 4, 513-527.

Rebesco, M., Stow, D. 2001. Seismic expression of contourites and related deposits: a preface. Mar. Geophys. Res. 22, 303-308.

Rebesco, M., Hernández-Molina, F.J., Van Rooij, D., Wåhlin, A., 2014. Contourites and associated sediments controlled by deep-water circulation processes: state of the art and future considerations. Mar. Geol. 352, 111-154.

Reddy, M., 2001. Descriptive Physical Oceanography. A.A Balkema Publishers, 445.

Reid, J.L., 1979. On the contribution of the Mediterranean Sea out flow to the Norwegian- Greenland Sea. Deep-Sea Res. 26 (A), 1199-1223.

Ribeiro, A., 2013. Evolução geodinâmica de Portugal, os ciclos Meso Cenozóicos. In: Dias, R., Araújo, A., Terrinha, P., Kullberg, J.C. (Eds.), Geologia de Portugal, Volume II: Geologia Meso-cenozóica de Portugal, Escolar Editora, Lisboa, III 9-26.

Ribeiro, A., Kullberg, M.C., Kullberg, J.C., Manuppella, G., Phipps, S., 1990. A review of Alpine tectonics in Portugal: Foreland detachment in basement and cover rocks. Tectonophysics 184 (3-4), 357-366.

Rodrigues, S., 2017. Seismostratigraphic model of the Sines Contourite Drift (SW Portuguese margin) - depositional evolution, structural control and paleoceanographic implications. MSc Thesis, University of Lisbon, Lisbon.

Rogerson, M., Rohling, E., Weaver, P., Murray, J., 2005. Glacial to interglacial changes in the settling depth of the Mediterranean Outflow plume. Paleoceanography 20 (3), 1-12.

Rogerson, M., Rohling, E., Weaver, P. 2006. Promotion of meridional overturning by Mediterranean-derived salt during the last deglaciation. Paleoceanography 21, 1-8.

Rogerson, M., Rohling, E., Bigg, G.R., Ramirez, J., 2012. Paleoceanography of the Atlantic-Mediterranean exchange: Overviewand first quantitativeassessment of climatic forcing. Rev. Geophys. 50, 1-32.

Roque, C., Duarte, H., Terrinha, P., Valadares, V., Noiva, J., Cachão, M., Ferreira, J., Legoinha, P., Zitellini, N., 2012. Pliocene and Quaternary depositionalmodel of the Algarve margin contourite drift (Gulf of Cadiz, SW Iberia): seismic architecture, tectoni control and paleoceanographic insights. Mar. Geol. 303-306, 42-62.

Roque, D., Parras-Berrocal, I., Bruno, M., Sánchez-Leal, R., Hernández-Molina, F.J., 2019. Seasonal variability of intermediate water masses in the Gulf of Cádiz: implications of the Antarcic and subarctic seesaw. Ocean Sci. 15, 1381-1397.

Rosas, F., Duarte, J., Terrinha, P., Valadares, V., Matias, L., Gutscher, M.A., 2009. Major bathymetric lineaments and soft sediment deformation in NW gulf of Cadiz (Africa-Iberia plate boundary): new insights from high resolution multibeam bathymetry data and analogue modelling experiments. Mar. Geol. 261 (1-4), 33-47.

Rovere, M., Pellegrini, C., Chiggiato, J., Campiani, E., Trincardi, F., 2019. Impact of dense bottom water on a continental shelf: An example from the SW Adriatic margin. Mar. Geol. 408, 123-143.

Schönfeld, J., Zahn, R., 2000. Late Glacial to Holocene history of the Mediterranean Outflow. Evidence from benthic foraminiferal assemblages and stable isotopes at the Portuguese margin. Palaeogeogr. Palaeoclimatol. Palaeoecol. 159, 85-111.

Serra, C.S., Martínez-Loriente, S., Gràcia, E., Urgeles, R., Vizcaino, A., Perea, H., Bartolome, R., Pallàs, R., Iacono, C.L., Diez, S., Dañobeitia, J., Terrinha, P., Zitellini, N., 2020. Tectonic evolution,

geomorphology and influence of bottom currents along a large submarine canyon system: The São Vicente Canyon (SW Iberian margin). Mar. Geol. 426, 106219.

Sierro, F.J., Glez Delgado, J.A., Dabrio, C., Flores, J.A., Civis, J., 1991. The Neogene of the Guadalquivir basin. Paleontologia y Evolució Mem. Especial 2: Iberian Neogene basins, 209-250.

Sierro, F.J., Ledesma, S., Flores, J.A., 2008. Astrobiochronology of late neogene deposits near the strait of Gibraltar (SW Spain). Implications for the tectonic control of the messinian salinity crisis. In: Biand, F. (Ed.), The messinian salinity crisis from mega-deposits to microbiology, CIESM workshop monographs, Monaco, 45-48.

Sierro, F.J., Hodell, D.A., Andersen, N., Azibeiro, L.A., Jimenez-Espejo, F.J., Bahr, A., Flores, J.A., Ausin, B., Rogerson, M., Lozano-Luz, R., Lebreiro, S., Hernández-Molina, F.J., 2020. Mediterranean Overflow over the last 250 ky. Freswater forcing from the tropics to the ice sheets. Paleoceanogr. Paleoclimatol. (in press).

Stow, D.A.V., Faugères, J.-C., 2008. Contourites facies and the facies model. In: Rebesco, M., Camerlenghi, A. (Eds.), Contourites. Dev. Sedimentol. Elsevier, Amsterdam, 60, 223-256.

Stow, D., Hunter, S., Wilkinson, D., Hernández-Molina, F., 2008. The nature of contourite deposition, In: Rebesco, M. Camerlenghi, A. (Eds.), Contourites. Dev. Sedimentol. Elsevier, Amsterdam, 60, 143-156.

Stow, D.A.V., Hernández-Molina, F.J., Llave, E., Bruno, M., García, M., Díaz del Río, V., Somoza, L., Brackenridge, R.E., 2013. The Cadiz contourite channel: sandy contourites, bedforms and dynamic current interaction. Mar. Geol. 343, 99-114.

Talley, L., McCartney, M., 1982. Distribution and circulation of Labrador Sea water. J. Phys. Oceanogr. 12 (11), 1189-1205.

Teixeira, M., Terrinha, P., Roque, C., Rosa, M., Ercilla, G., Casas, D., 2019. Interaction of alongslope and downslope processes in the Alentejo Margin (SW Iberia) – Implications on slope stability. Mar. Geol. 410, 88-108.

Teixeira, M., Terrinha, P., Roque, C., Voelker, A., Silva, P., Salgueiro, E., Abrantes, F., Naughton, F., Mena, A., Ercilla, G., Casas, D., 2020. The Late Pleistocene-Holocene sedimentary evolution of the Sines 1 Contourite Drift (SW Portuguese Margin): A multiproxy approach. Sed. Geol. (in press).

Terrinha, P., Pinheiro, L.M., Henriet, J.-P., Matias, L., Ivanov, M.K., Monteiro, J.H., Akhmetzhanov, A., Volkonskaya, A., Cunha, T., Shaskin, P., Rovere, M., 2003. Tsunamigenic-seismogenic structures, neotectonics, sedimentary processes and slope instability on the southwest Portuguese margin. Mar. Geol. 195, 55-73.

Terrinha, P., Rocha, R.B., Rey, J., Cachão, M., Moura, D., Roque, C., Martins, L., Valadares, V., Cabral, J., Azevedo, M.R., Barbero, L., Clavijo, E., Dias, R.P., Matias, H., Matias, L., Madeira, J., Silva, C.M., Munhá, J.R., Rebelo, L., Ribeiro, C., Vicente, J., Noiva, J., Youbi, N., Bensalah, M. K., 2013a. A Bacia do Algarve: Estratigrafia, Paleogeografia e Tectónica. In: Dias, R., Araújo, A., Terrinha, P., Kullberg, J.C. (Eds.), Geologia de Portugal, Volume II: Geologia Meso-cenozóica de Portugal, Escolar Editora, Lisboa, III.1., 29-166.

Terrinha, P, Matias, L., Valadares, V., Roque, C., Duarte, J., Rosas, F., Silva, S., Cunha, T., Batista, L., Duarte, H., Garrara, G., Gràcia, E., Zitellini, N., Lourenço, N., Pinto de Abreu, M., 2013b. A Margem Sul Portuguesa Profunda. In: Dias, R., Araújo, A., Terrinha, P., Kullberg, J.C. (Eds.), Geologia de Portugal, Volume II: Geologia Meso-cenozóica de Portugal, Escolar Editora, Lisboa, III.2., 167-194.

Thran, A.C., Dutkiewicz, A., Spence, P., Müller, R.D., 2018. Controls on the global distribution of contourite drifts: Insights from an eddy-resolving ocean model. Earth Planet. Sci. Lett. 489, 228-240.

Toucanne, S., Mulder, T., Schönfeld, J., Hanquiez, V., Gonthier, E., Duprat, J., Cremer, M., Zaragosi, S., 2007. Contourites of the gulf of Cadiz: a high-resolution record of the paleocirculation of the Mediterranean outflow water during the last 50,000 years. Palaeogeogr. Palaeoclimatol. Palaeoecol. 246, 354-366.

Tucholke, B.E., Sawyer, D.S., Sibuet, J.C., 2007. Breakup of the Newfoundland Iberia rift. In: Karner, G.D., Manatschal, G., Pinheiro, L.M. (Eds.), Imaging, Mapping and Modelling Continental Lithosphere Extension and Breakup. Geol. Soc. London Spec. Publ. 282 (1), 9-46.

Van Rooij, D., Blamart, D., Kozachenko, M., Henriet, J.-P., 2007. Small mounded contourite drifts associated with deep-water coral banks, Porcupine Seabight, NE Atlantic Ocean. In: Viana, A., Rebesco, M. (Eds.), Economic and Paleoceanographic Importance of Contourites. Geol. Soc. London Spec. Publ. 276, 225-244.

Van Rooij, D., Iglesias, J. Hernández-Molina. F.J., Ercilla, G., Gomez-Ballesteros, M., Casas, D., Llave, E., De Hauwere, A., Garcia-Gil, S., Acosta, J., Henriet, J.-P., 2010. The Le Danois Contourite Deositional System: Interactions between the Mediterranean Outflow Water and the upper Cantabrian slope (North Iberian margin). Mar. Geol. 274 (1-4), 1-20.

Vanney, J.R., Mougenot, D., 1981. La Plate-forme Continentale du Portugal et les Provinces adjacentes: Analyse Geomorphologique. Memórias dos Serviços Geológicos de Portugal, Lisboa, 28, 86.

Viana, A., 2002. Seismic expression of shallow- to deep-water contourites along the south-eastern Brazilian margin. Mar. Geophys. Res. 22, 509-521.

Voelker, A.H.L., Lebreiro, S.M., Schönfeld, J., Cacho, I., Erlenkeuser, H., Abrantes, F., 2006. Mediterranean outflow strengthening during northern hemisphere coolings: a salt source for the glacial Atlantic? Earth Planet. Sci. Lett. 245 (1-2), 39-55.

Voelker, A.H.L., Salgueiro, E., Rodrigues, T., Jimenez-Espejo, F., Bahr, A., Alberto, A., Loureiro, I., Padilha, M., Rebotim, A., Röhl, U., 2015. Mediterranean Outflow and surface water variability off southern Portugal during the early Pleistocene: A snapshot at Marine Isotope Stages 29 to 34 (1020-1135 Ka), Glob. Planet. Chang.133, 223-237.

Yin, S., Hernández-Molina, F.J. Zhang, W., Li, J., Wang, L., Ding, W., Ding, W., 2019. The influence of oceanographic processes on contourite features: A multidisciplinary study of the northern South China Sea. Mar. Geol. 415, 105967.

Zenk, W., 1970. On the temperature and salinity structure of the Mediterranean water in the Northeast Atlantic. Deep-Sea Res. 17, 627-631.

Zenk, W., 1975. On the Mediterranean outflow west of Gibraltar. Meteor Forschungsergebnisse, Deutsche Forschungsgemeinschaft, Reihe A Allgemeines, Physik und Chemie des Meeres, Gebrüder Bornträger, Berlin, Stuttgart, A16, 23-34.

Zhang, W., Hanebuth, T.J.J., Stöber, U., 2016a. Short-term sediment dynamics on a meso-scale contourite drift (off NW Iberia): Impacts of multi-scale oceanographic processes deduced from the analysis of mooring data and numerical modelling. Mar. Geol. 378, 81-100.

Zitellini, N., Mendes, L.A., Cordona, D., Danobeitia, J., Nichols, R., Pellis, G., Ribeiro, A., Sartori, R., Torelli, L., Bartolome, R., Bortoluzzi, G., Calafato, A., Carrilho, F., Casoni, L., Chierici, F., Corela, C., Correggari, A., Vedova, B.D., Gracia, E., Jornet, P., Landuzzi, M., Ligi, M., Magagnoli, A., Marozzi, G., Matias, L., Penitenti, D., Rodriguez, P., Rovere, M., Terrinha, P., Vigliotti, L., Ruiz, A.Z., 2001. Source of 1755 Lisbon earthquake and tsunami investigated. Eos Trans. AGU 82 (26), 290-291.

Zitellini, N., Rovere, M., Terrinha, P., Chierici, F., Matias, L., BIGSETS Team, 2004. Neogene Through Quaternary Tectonic Reactivation of SW Iberian Passive Margin. Pure Appl. Geophys. 161 (3), 565-587.

Zitellini, N., Gràcia, E., Matias, L., Terrinha, P., Abreu, M.A., DeAlteriis, G., Henriet, J.P., Dañobeitia, J.J., Masson, D.G., Mulder, T., Ramella, R., Somoza, L., Diez, S., 2009. The quest for the Africa-Eurasia plate boundary west of the Strait of Gibraltar. Earth Planey. Sci. Lett. 280 (1-4), 13-50.
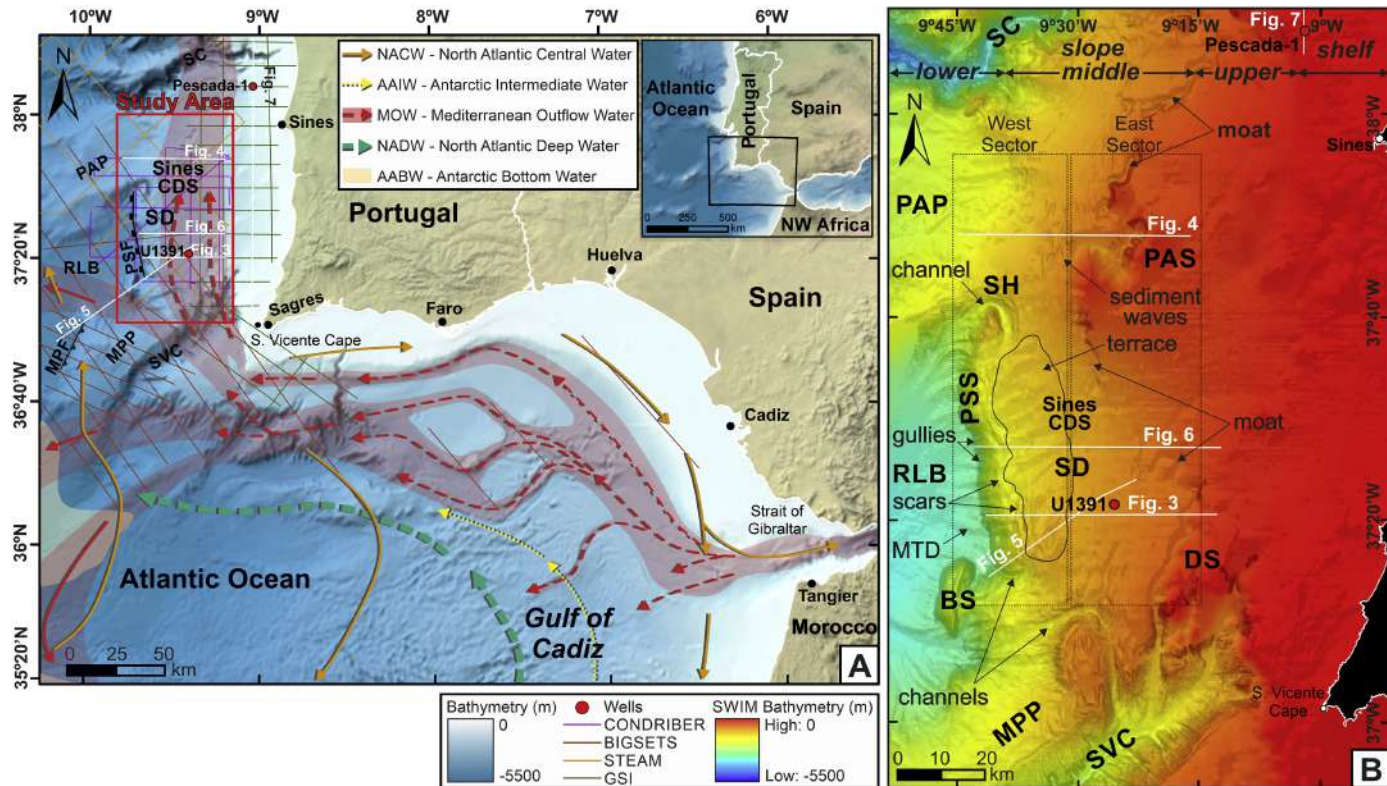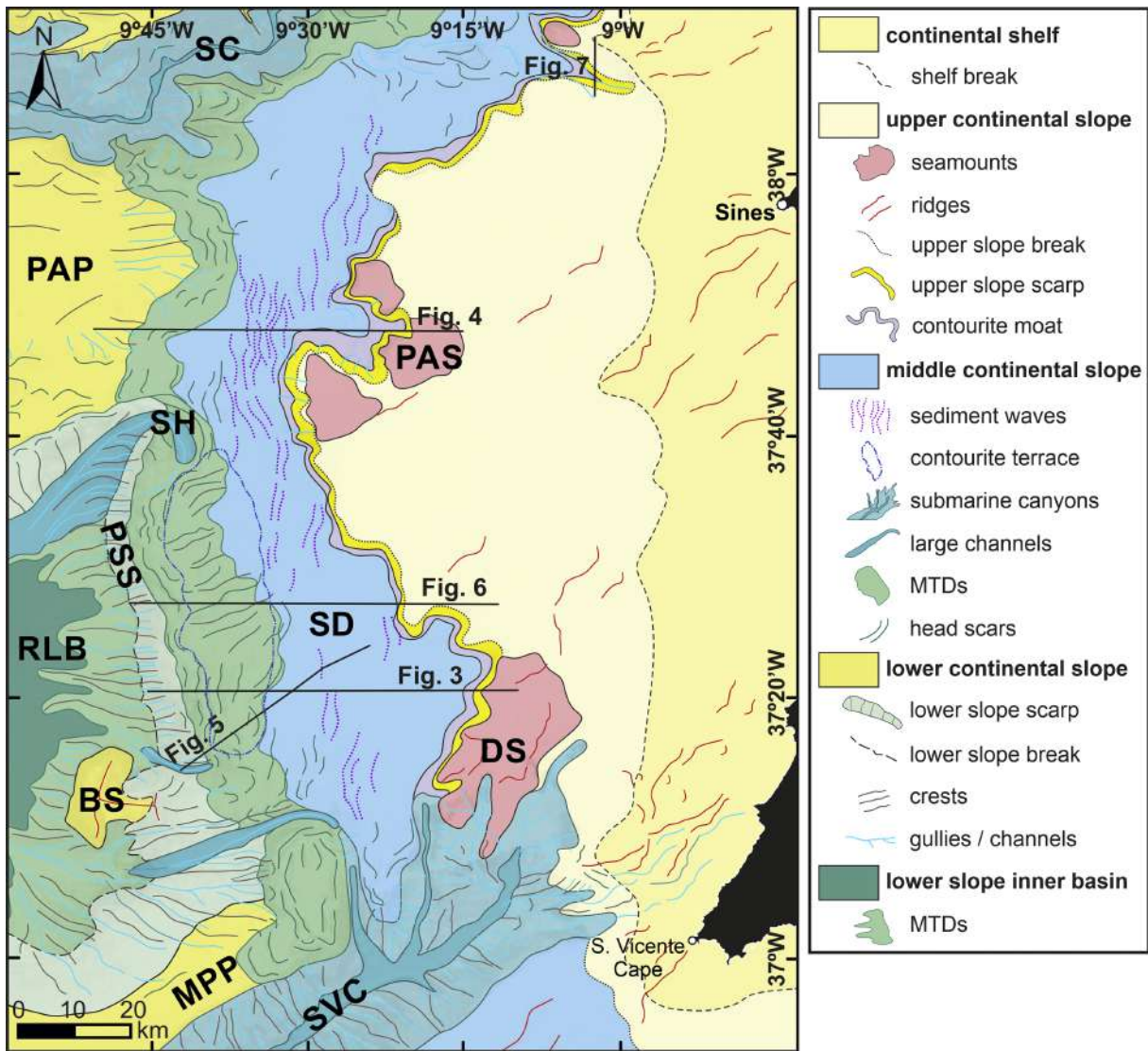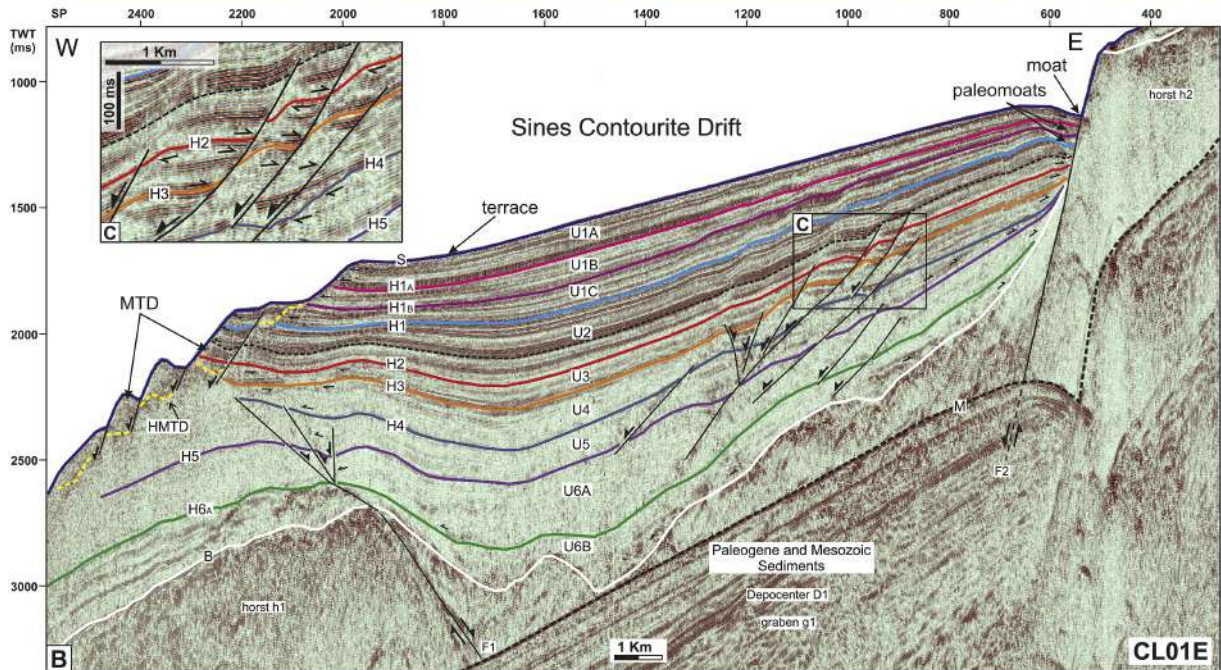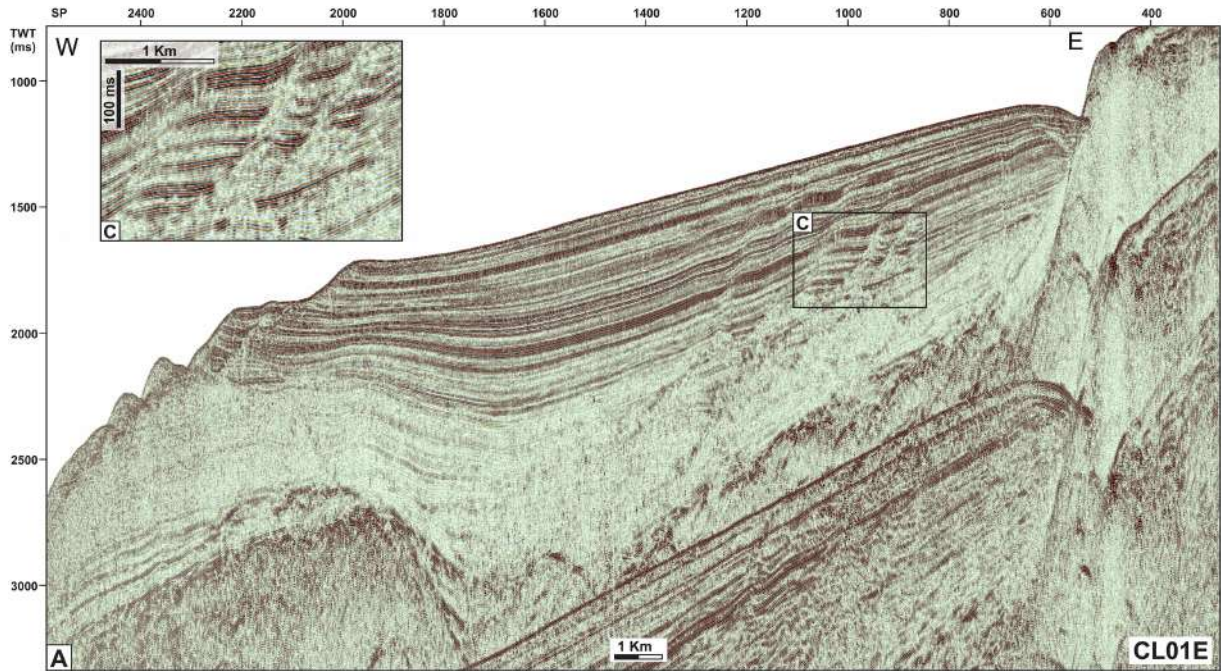
Figure 1

Figure 2

Figure 3
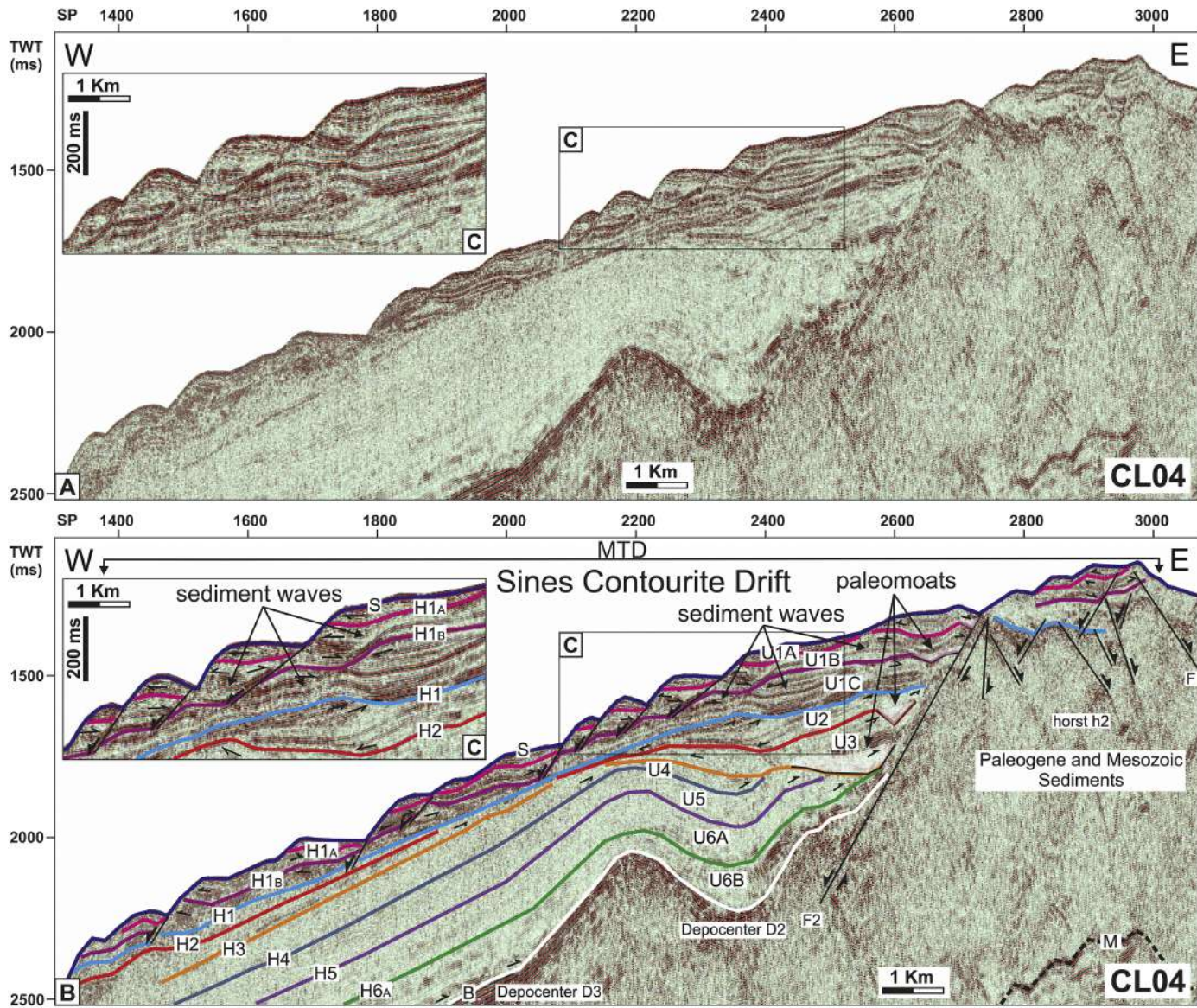
Figure 4
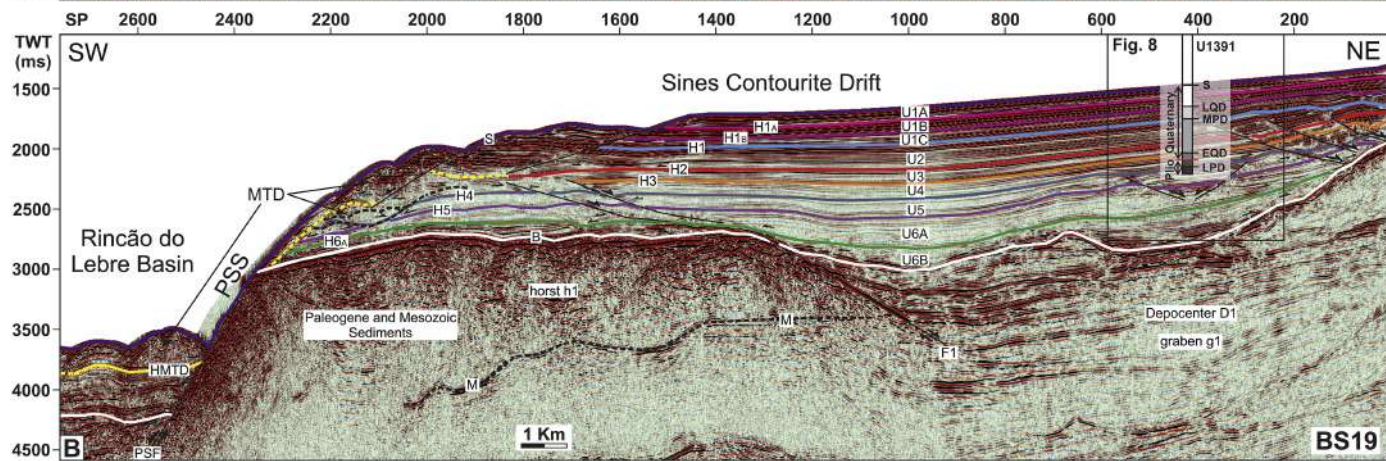
Figure 5

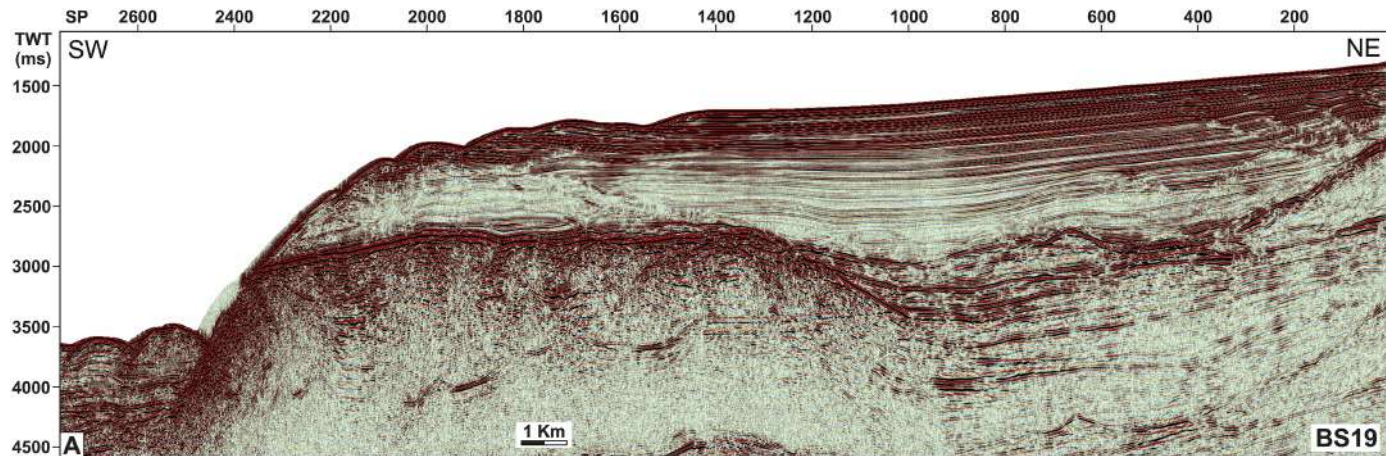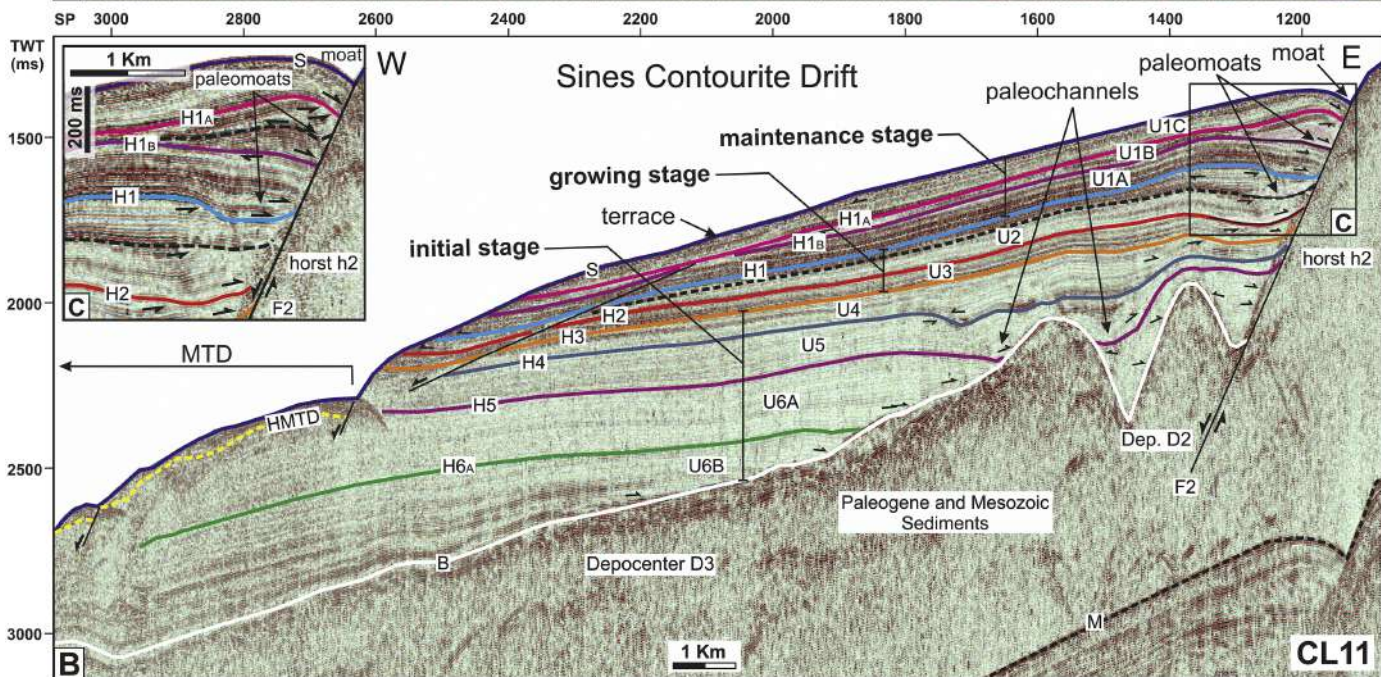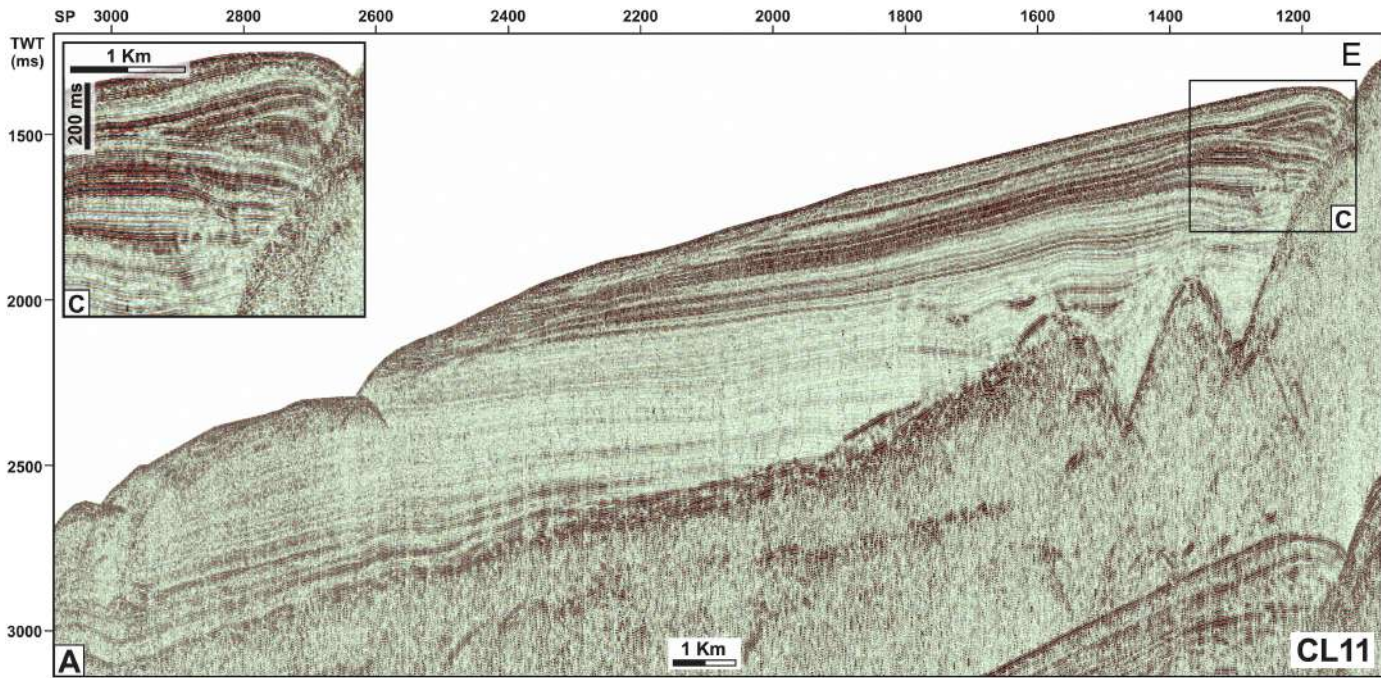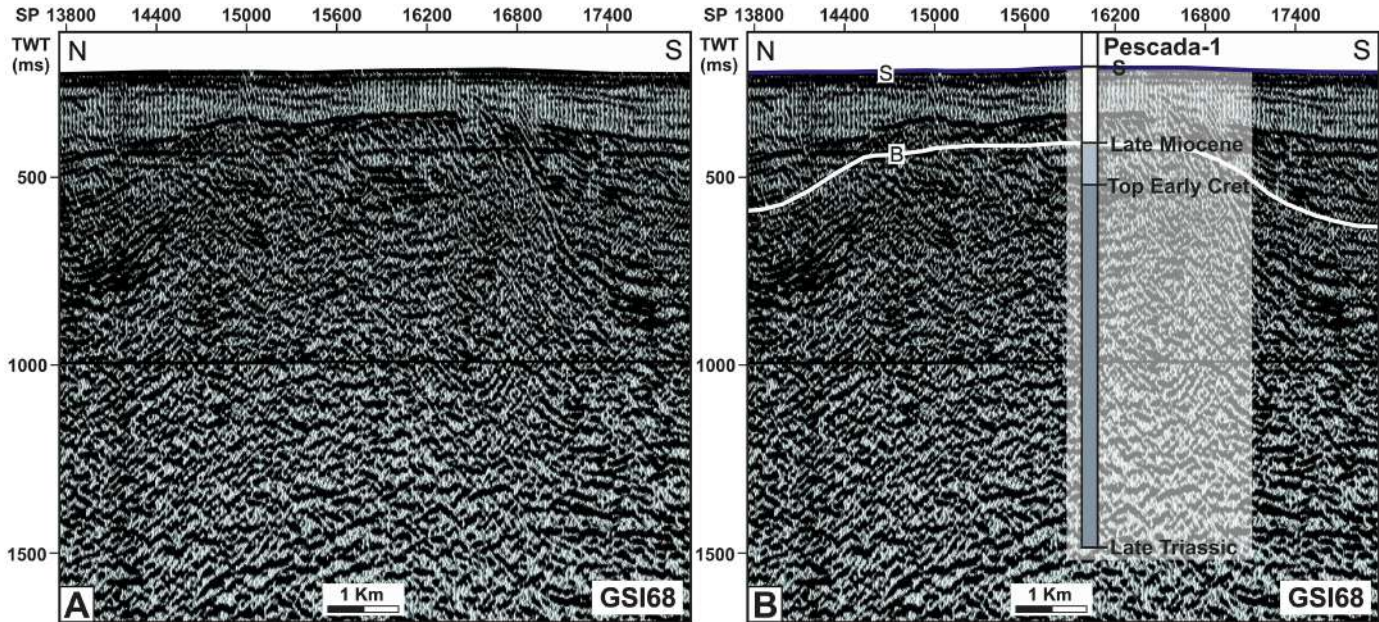Figure 6

Figure 7
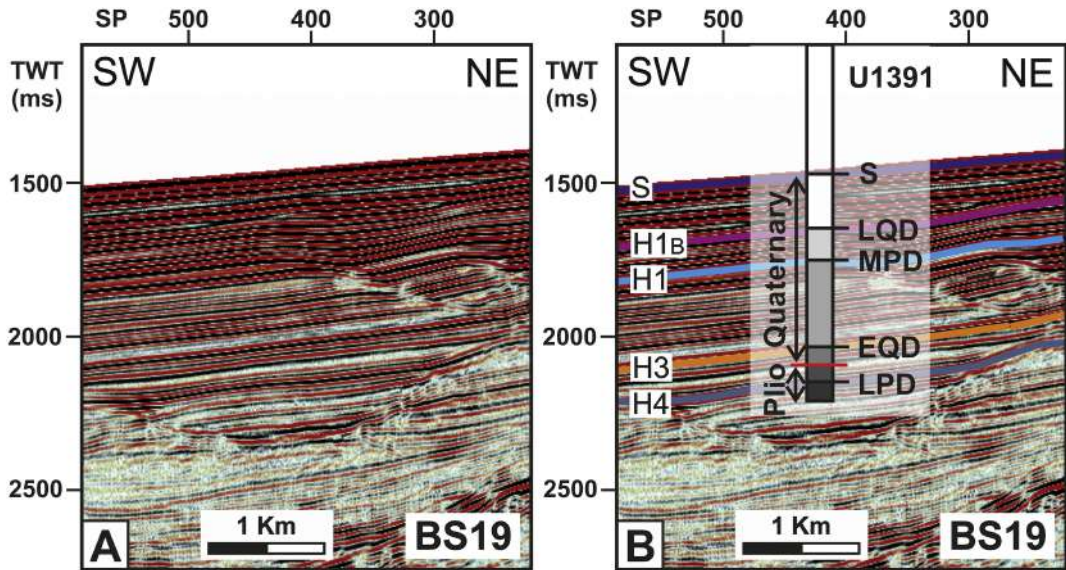
Figure 8
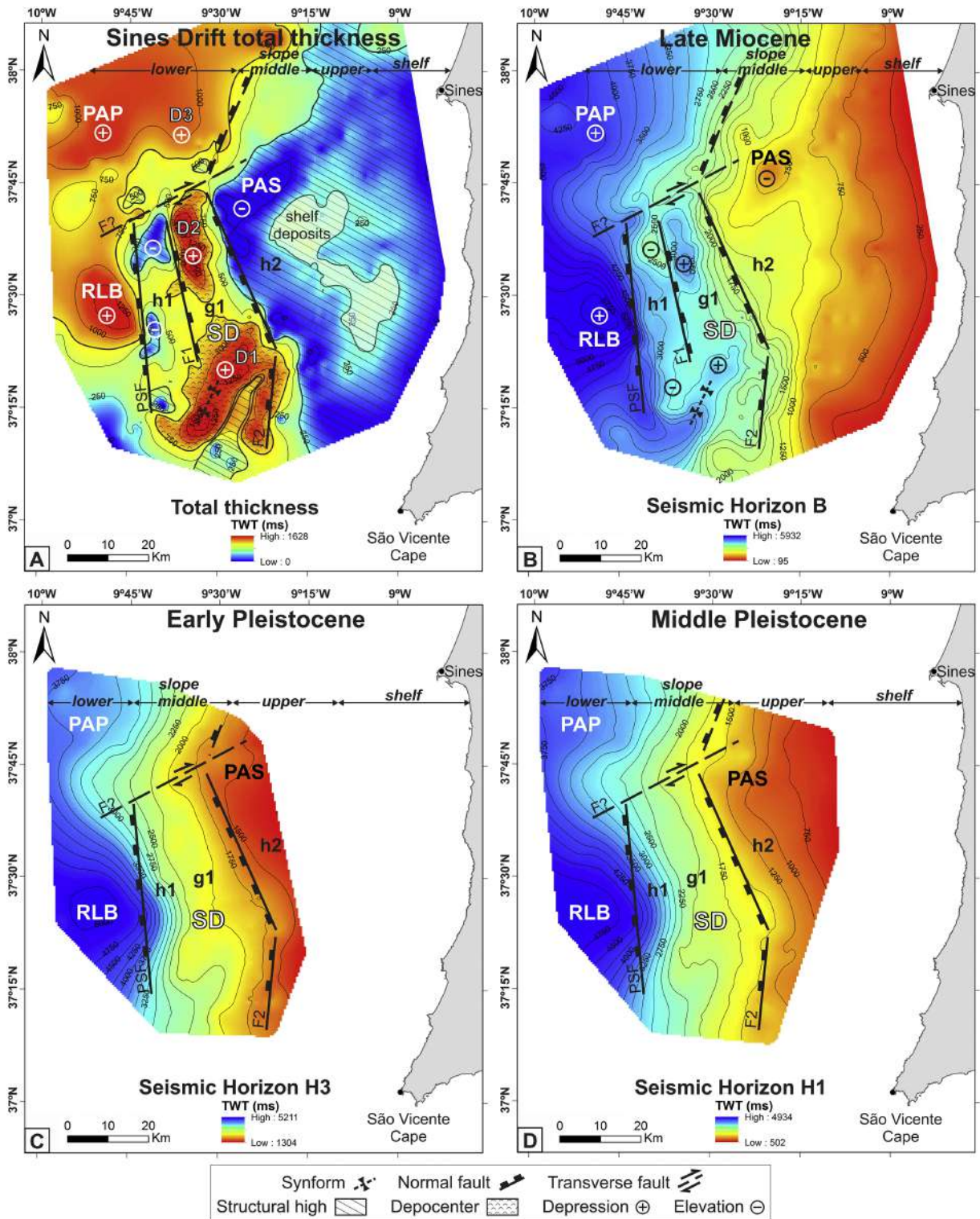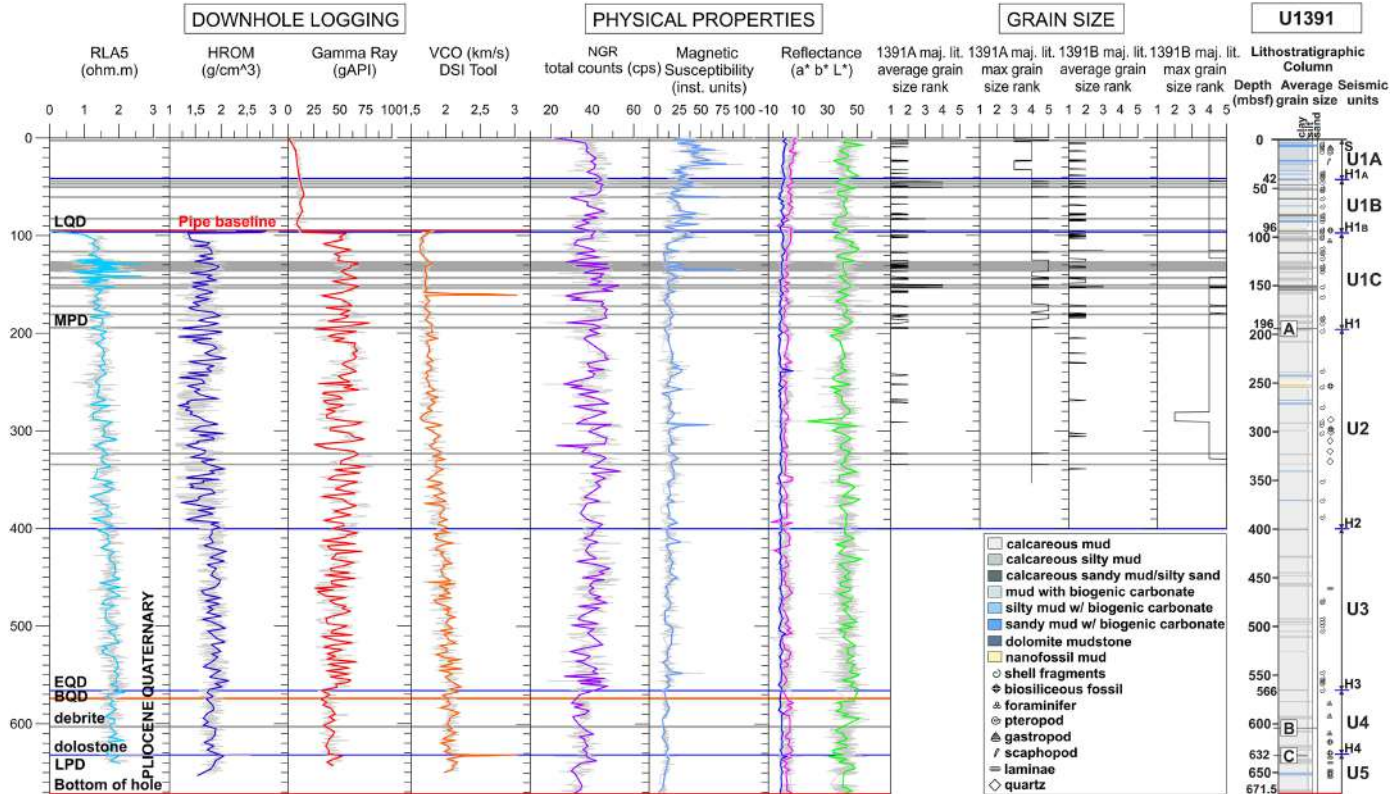
Figure 9

Figure 10

U1391A-22X-4-A

(processed)

193.5

A

calcareous mud

calcareous silty mud

calcareous sandy mud

bigradational sequence

194.7

calcareous silty mud

U1391C-30R-1-A

(processed)

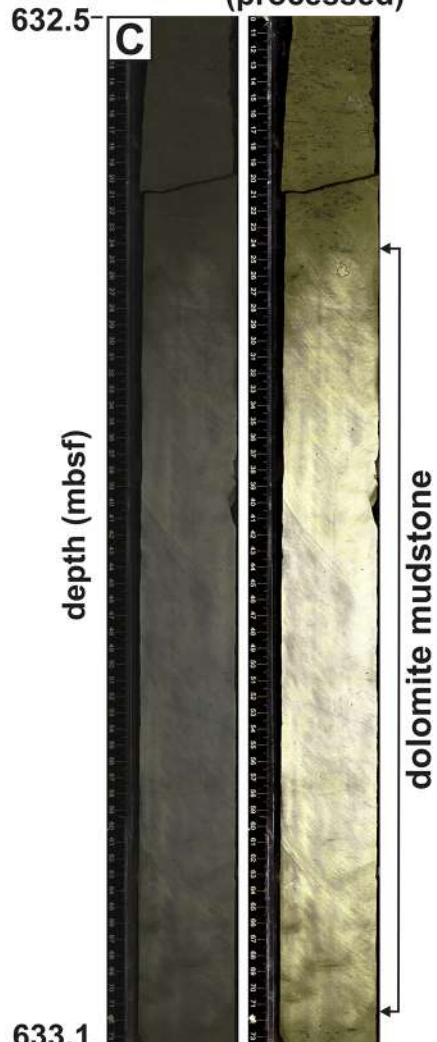604.4

B
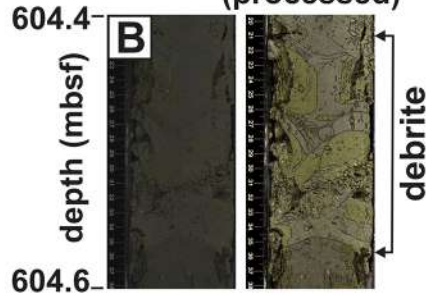
depth (mbsf)

debrite

604.6

U1391C-32R-7-A

(processed)

632.5

C

depth (mbsf)

dolomite mudstone

633.1
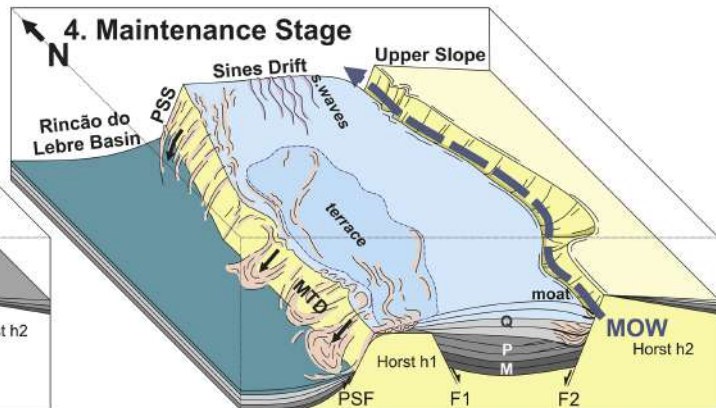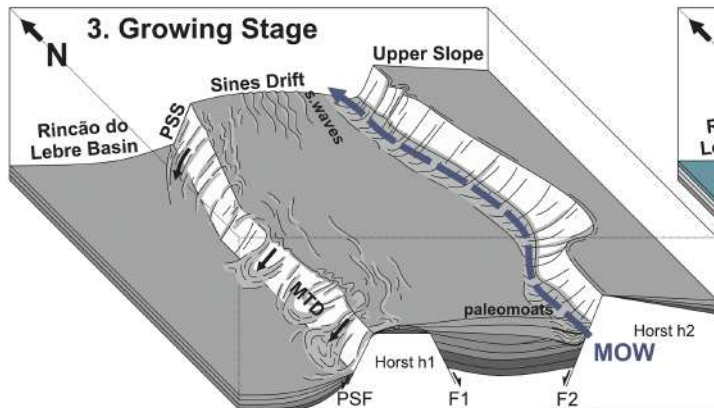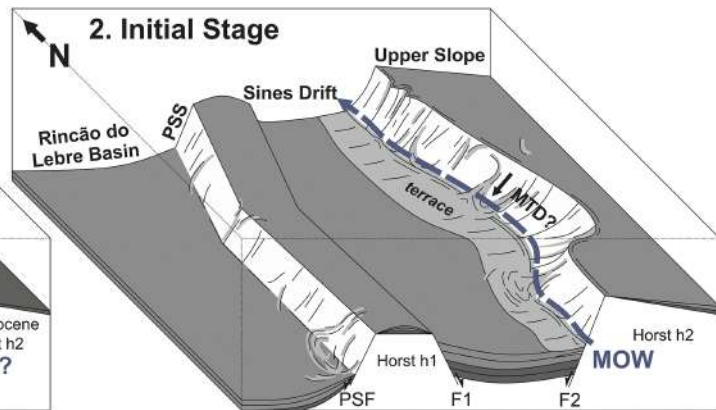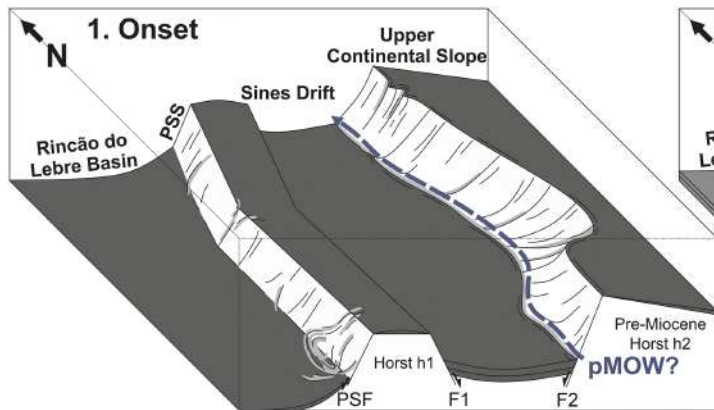
Figure 11
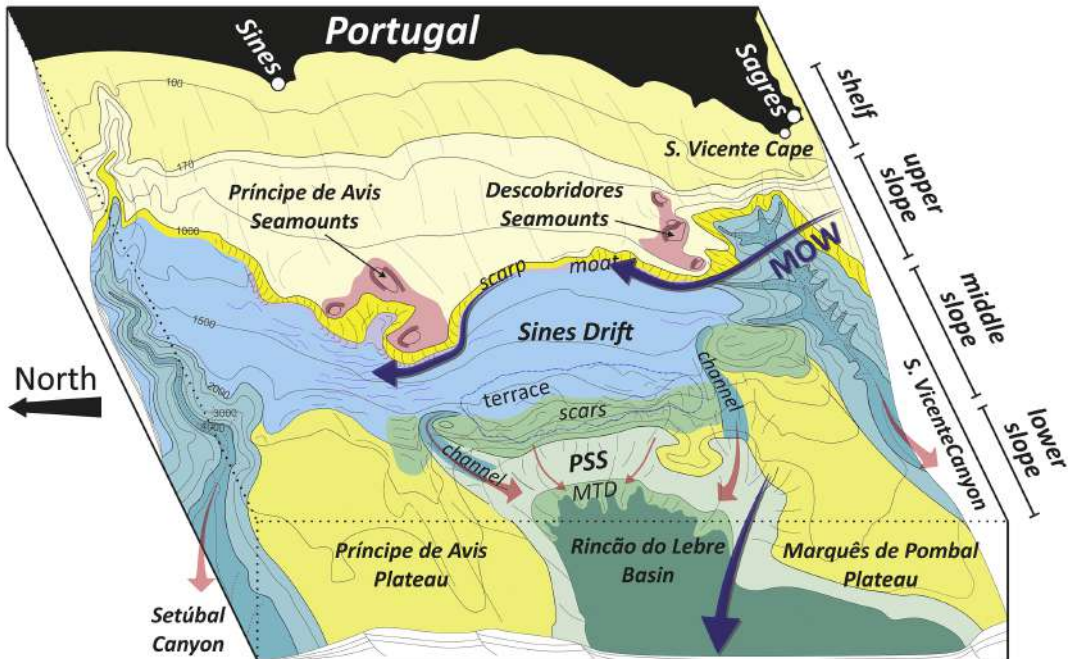
Figure 12

Figure 13

Figure 14

A **Type 1:**
sheet to wedge plastered drift
topped by a terrace in proximal sector

slope

terrace
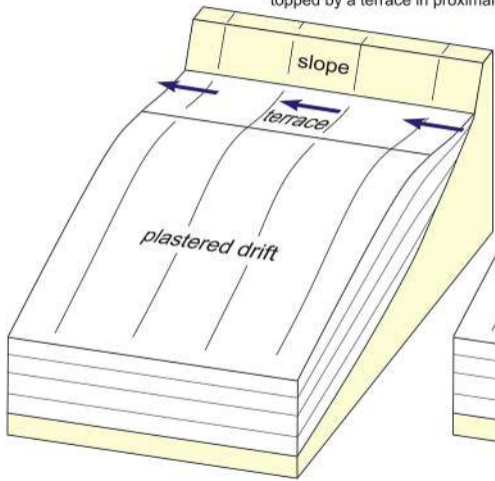
plastered drift

B **Type 2:**
lens to mounded plastered drift
with an adjacent U-shaped moat

slope

moat

plastered drift

paleomoats
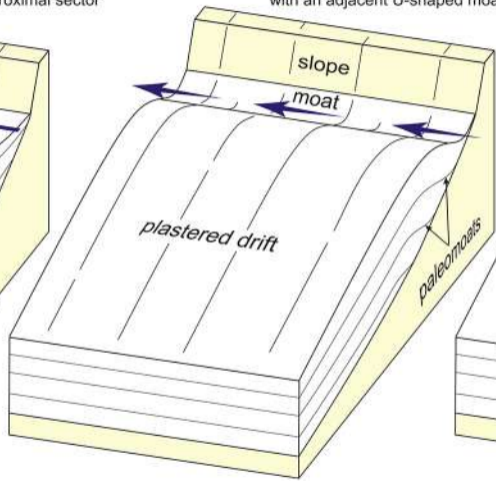
C **Type 3:**
tabular, concave plastered drift
and adjacent V-shaped moat

slope

moat

plastered drift

Figure 15